PNNL-26750

Pacific Northwest
NATIONAL LABORATORY
Proudly Operated by Battelle Since 1965

Al/Zr/U-10Mo Foil Sensitivity Analyses

August 2017

BN Nguyen
CH Henager, Jr.
CA Lavender
KL Simmons

U.S. DEPARTMENT OF ENERGY

Prepared for the U.S. Department of Energy
under Contract DE-AC05-76RL01830

DISCLAIMER

PACIFIC NORTHWEST NATIONAL LABORATORY
operated by
BATTELLE
for the
UNITED STATES DEPARTMENT OF ENERGY
under Contract DE-AC05-76RL01830

Printed in the United States of America

Available to DOE and DOE contractors from the Office of Scientific and Technical Information,
P.O. Box 62, Oak Ridge, TN 37831-0062
www.osti.gov
ph: (865) 576-8401
fax: (865) 576-5728
email: reports@osti.gov

Available to the public from the National Technical Information Service
5301 Shawnee Rd., Alexandria, VA 22312
ph: (800) 553-NTIS (6847)
or (703) 605-6000
email: info@ntis.gov
Online ordering: http://www.ntis.gov

PNNL-26750

Al/Zr/U-10Mo Foil Sensitivity Analyses

BN Nguyen
CH Henager, Jr.
CA Lavender
KL Simmons

August 2017

Prepared for
the U.S. Department of Energy
under Contract DE-AC05-76RL01830

Pacific Northwest National Laboratory
Richland, Washington 99352

Abstract

This report describes modeling work performed to analyze typical uranium (U)-10 wt% molybdenum (Mo) foils co-rolled with zirconium (Zr) and clad in aluminum (Al). The purpose of the analyses was to predict foil integrity, while accounting for the mechanical properties, thickness, and roughness of the Zr-layer coating. First, plane-strain ABAQUS® finite element (FE) models of the U-10Mo foils with a Zr diffusion barrier clad in Al subjected to uniform bending were developed. These models contain two symmetric Zr layers perfectly and smoothly bonded to the U-10Mo and Al layers. A sensitivity study using ABAQUS was conducted considering four thickness values and three assumed stress-strain behaviors of the Zr layer. The assumed Zr behaviors reflect the oxygen (O_2) content in Zr that represents nearly pure Zr, low-O_2-content Zr (e.g., ≤ 30 (wt ppm)$^{1/2}$), and high-O_2-content Zr (e.g., ≥ 100 (wt ppm)$^{1/2}$). An elastic-plastic damage model was employed in ABAQUS to describe the deformation and damage of all the materials in the foils. The results from this analysis help elucidate the effects of the Zr thickness and stress-strain behavior on the foil deformation and integrity during uniform bending. Next, a FE model involving asperities (interface roughness) along all the interfaces of a 1 mm thick Al/Zr/U-10Mo foil was built and analyzed for uniform bending to compare with the model with smooth interfaces considering a typical behavior of Zr. These analyses show an important effect of the interface roughness on foil integrity, because damage concentrations created at the asperities developed into microcracks propagating in the U-10Mo core layer. Finally, to further investigate the roughness effect, the foil model with interface roughness and subjected to the cantilever beam loading configuration was analyzed considering three given stress-strain behaviors of Zr. These analyses indicate that, with increasing deflection, damage accumulations found at and near the clamped extremity of the foils, particularly at the asperities along the Zr/U-10Mo interfaces, propagated in the U-10Mo core layer. The foil with the highest O_2 content suffered the most from crack propagation into the U-10Mo core during bending.

Summary

This work reported here was conducted to support efforts of the U.S. Department of Energy National Nuclear Security Administration's Office of Material Management and Minimization to develop a low-enriched fuel for U.S. high-power research reactors. The material under investigation is a uranium-10 wt% molybdenum (U-Mo) alloy fuel co-rolled with zirconium (Zr) and clad in aluminum (Al). This report describes modeling work performed to analyze typical Al/Zr/U-10Mo foils to predict foil integrity, accounting for the mechanical properties, thickness, and roughness of the Zr-layer coating.

The impact of the Zr/U-Mo interface on foil formability is an important problem that needs to be addressed to guide foil fabrication. The objective of this work was to develop models to parametrically study the Zr/U-Mo interface to understand the effects of foil processing on foil formability and cracking. In this sensitivity study, we investigated the effects of Zr-layer thickness and mechanical properties as well as the effect of the interface roughness on foil deformation and integrity. For this purpose, in the first round of analyses, finite element (FE) models with smooth interfaces of the cross sections of 1 mm thick foils containing a 0.66 mm thick U-10Mo core and two symmetric Al and Zr layers were developed for foil analyses using the ABAQUS® FE package. The total thickness of the Al/Zr/U-10Mo foil and the thickness of the U-10Mo core were kept constant, but the thickness of the Zr layer was varied to achieve uniformly thick 4-, 10-, 25-, and 37-micron Zr layers. All the layers were assumed to be perfectly bonded. The analyses used combined published and assumed constitutive mechanical data for the constituent layers. In addition, by exploring Pacific Northwest National Laboratory's Vickers hardness data for Zr with different levels of O_2 content, and considering three possible behaviors of Zr covering the range from nearly zero to high O_2 contents, a conceptual envelope of the stress-strain responses of Zr was proposed and used in the analyses. The elastic-plastic damage model with isotropic hardening and isotropic damage of the ABAQUS constitutive laws was used to simulate the deformation of the foil models subjected to uniform bending to achieve the permanent curvature radius of 76.58 mm after springback.

In the second round of analyses, from a microstructural image of an actual foil cross section and using the National Institute of Standards and Technology's OOF2 software, a foil model with rough interfaces was developed to study the effect of the interface asperities on the mechanical response and integrity of a deformed foil. Comparative analyses using the foil models with smooth and rough interfaces subjected to uniform bending were performed to elucidate the impact of the interface roughness on foil integrity. Finally, to further study this effect, the foil model with rough interfaces was analyzed under a cantilever beam bending configuration using the above assumed behaviors of the Zr layers. The conclusions drawn from this work are as follows:

- *The Zr stress-strain behavior* has an important effect on the foil's deformation and integrity. The very *high strength* but *brittle* Zr due to high O_2 content induced very high stresses that caused failure of the Zr layers. With the use of a high O_2-content Zr, higher stress concentrations were also found along the interfaces between the Zr and U-10Mo layers causing plastic deformation in these regions, although the U-10Mo core away from the interfaces was still elastic. The use of ductile Zr materials (with low O_2 contents) is very important for reducing stress concentrations and improving the integrity and deformation behavior of foils.
- *The effect of the Zr-layer thickness* on the stress and strain distributions is more significant at springback than at the maximum applied moments. However, for the values of the Zr thickness considered, the Zr thickness effect appears to be less important than the effects of the Zr mechanical properties and interface roughness, and therefore would not be a concern for foil fabrication.

- Interface roughness has an important impact on foil integrity; the analyses using the model with rough interfaces show that the asperities along the interfaces are sites of stress, strain, and damage concentrations. Under a critical loading mode (e.g., cantilever beam loading), damage localization in these sites could develop microcracks propagating into the U-10Mo core. Therefore, minimizing the interface roughness would improve the foil's mechanical integrity.

Because the sensitivity analyses performed under this effort used assumed or published data in model foils, the results have indicative and qualitative values. However, the modeling capability established can be enhanced and applied to simulate actual tests based on measured data that could be planned in future work to effectively guide foil fabrication.

Acknowledgments

This work was funded by the U.S. Department of Energy National Nuclear Security Administration's Office of Material Management and Minimization and performed at Pacific Northwest National Laboratory under contract DE-AC05-76RL01830.

Acronyms and Abbreviations

Al	aluminum
FE	finite element
Mo	molybdenum
NIST	National Institute of Standards and Technology
O_2	oxygen
U	uranium
Zr	zirconium

Contents

Abstract iii
Summary v
Acknowledgments vii
Acronyms and Abbreviations ix
1.0 Introduction 1
2.0 Finite Element Models of Al/Zr/U-10Mo Foils 1
2.1 FE Models with Smooth Interfaces 1
2.2 A FE Model with Rough Interfaces 3
3.0 Mechanical Properties 4
4.0 Results and Discussions 8
4.1 Effects of Zr-Layer Thickness and Mechanical Properties 8
4.2 Effect of Interface Roughness 26
5.0 Conclusions 35
6.0 References 36

Figures

1 (a) Illustration of a Two-Dimensional FE Mesh of the Al/Zr/U-10Mo Foil with Smooth Interfaces, and (b) Snapshots Showing Detailed Meshes Containing Zr Layers of Different Thicknesses 2

2 (a) Boundary Conditions Applied to Deform the Al/Zr/U-10Mo Foil Involving a Uniform Applied Moment to Cause (b) the Permanent Deformed Configuration after Springback Achieving a Curvature Radius of 76.58 mm (3.015 in.) 3

3 A High-Resolution FE Model of the Al/Zr/U-10Mo Foil with Rough Interfaces 4

4 The True Stress-Strain Response of Al-6061-HIP-L1T1 Based on Idaho National Laboratory's Data 6

5 The Estimated Stress-Strain Response of U-10Mo Based on Rest et al. (2009) and Burkes et al. (2009)7

6 The Assumed Uniaxial Stress-Strain Behaviors of Zr for the Sensitivity Analysis 7

7 Contours of Von Mises Equivalent Stresses at the Maximum Applied Moment: Analysis for (a) Zr(1), (b) Zr(2), and (c) Zr(3) 9

8 Contours of Von Mises Equivalent Stresses in the Permanent Deformed Configuration after Springback Achieving a Curvature Radius of 76.58 mm: Analysis for (a) Zr(1), (b) Zr(2), and (c) Zr(3) 10

9 Contours of Equivalent Plastic Strains at the Maximum Applied Moments 13

10 Contours of Equivalent Plastic Strains in the Permanent Deformed Configuration after Springback Achieving a Curvature Radius of 76.58 mm 14

11 Damage Distributions at the Maximum Applied Moments 15

12 Damage Distributions in the Permanent Deformed Configuration after Springback Achieving a Curvature Radius of 76.58 mm 16

13 Through-Thickness Von Mises Equivalent Stress Distributions at the Maximum Applied Moments 17

14 Through-Thickness Von Mises Equivalent Stress Distributions after Springback 18

15 Through-Thickness Bending Stress Distributions at the Maximum Applied Moments 19

16 Through-Thickness Bending Stress Distributions after Springback 20

17 Through-Thickness Equivalent Plastic Strain Distributions at the Maximum Applied Moments 21

18 Through-Thickness Equivalent Plastic Strain Distributions after Springback 22

19 Through-Thickness Damage Indicator Distributions at the Maximum Applied Moments 23

20 Through-Thickness Damage Indicator Distributions after Springback 24

21 Contours of Von Mises Equivalent Stresses at the Maximum Applied Moment: Results from the Models with Smooth Interfaces (a) and with Interface Roughness (b) 27

22 Contours of Von Mises Equivalent Stresses after Springback: Results from the Models with Smooth Interfaces (a) and with Interface Roughness (b) 27

23 Contours of Equivalent Plastic Strains at the Maximum Applied Moment: Results from the Models with Smooth Interfaces (a) and with Interface Roughness (b) 28

24 Contours of Equivalent Plastic Strains after Springback: Results from the Models with Smooth Interfaces (a) and with Interface Roughness (b) 29
25 Damage Distributions at the Maximum Applied Moment: Results from the Models with Smooth Interfaces (a) and with Interface Roughness (b) 29
26 Damage Distributions after Springback: Results from the Models with Smooth Interfaces (a) and with Interface Roughness (b) 30
27 Boundary Conditions Applied to Deform the Al/Zr/U-10Mo Foil According to a Cantilever Beam Configuration 31
28 Snapshots of the Damage Distributions at the Clamped End Region Predicted by the Model with Interface Roughness for 4.5 mm Deflection 32
29 Snapshots of the Damage Distributions at the Clamped End Region Predicted by the Model with Interface Roughness for 5.5 mm Deflection 33
30 Snapshots of the Damage Distributions at the Clamped Region Predicted by the Models with (a) Smooth Interfaces and (b) Rough Interfaces for 5.5 mm Deflection 34
31 Example from an Experimental U-Mo Sample Showing Cracks Propagating from Asperities or Microvoids at an Interface 34

Tables

1 Mechanical Properties of the Foil Layers for Nonlinear FE Analyses 5
2 Summary of Al/Zr/U-10Mo Foil Model Features, Maximum Loading Levels, and Damage Predictions 25

1.0 Introduction

This work supports efforts of the U.S. Department of Energy National Nuclear Security Administration's Office of Material Management and Minimization to develop a low-enriched fuel for U.S. high-power research reactors. The material being investigated is a uranium-10 wt% molybdenum (U-Mo) alloy fuel co-rolled with zirconium (Zr) and clad in aluminum (Al). The modeling work performed to analyze typical Al/Zr/U-10Mo foils to predict foil integrity, accounting for the mechanical properties, thickness, and roughness of the Zr-layer coating, is described herein.

Sensitivity analyses of Al/Zr/U-Mo foil finite element (FE) models were performed using the ABAQUS® FE package (Dassault Systèmes 2016). The purpose of the analyses was to simulate the foil deformation under bending to identify the potential for fracturing the U-Mo core due to critical stress concentrations that could be generated from the interfaces between the U-Mo core and the Zr layers. This report describes the modeling work performed to analyze typical Al/Zr/U-10 Mo model foils to predict foil integrity accounting for the mechanical properties, thickness, and roughness of the Zr-layer coating.

2.0 Finite Element Models of Al/Zr/U-10Mo Foils

2.1 FE Models with Smooth Interfaces

To investigate the effects of the Zr coating thickness and mechanical properties on foil deformation and integrity, FE models of the cross sections of 1 mm thick foils containing a 0.66 mm thick U-10Mo core and two symmetric Al and Zr layers were developed for foil analyses using the ABAQUS FE package. The total thickness of the Al/Zr/U-10Mo foil and the thickness of U-10Mo core were kept constant, but the thickness of the Zr layer was varied to achieve 4-, 10-, 25- and 37-micron-thick Zr layers. All the thicknesses were uniform and perfect bonding was assumed between the layers. Figure 1a shows a two-dimensional FE mesh of an Al/Zr/U-10Mo foil cross section for plane-strain analysis. The external layers (in green color) are Al layers, while U-10Mo core is embedded in two Zr layers (colored in red). The entire length of the cross section is 12.73 mm wide. Figure 1b shows the details of the zoomed-in meshes from four FE models containing Zr layers of different thicknesses.

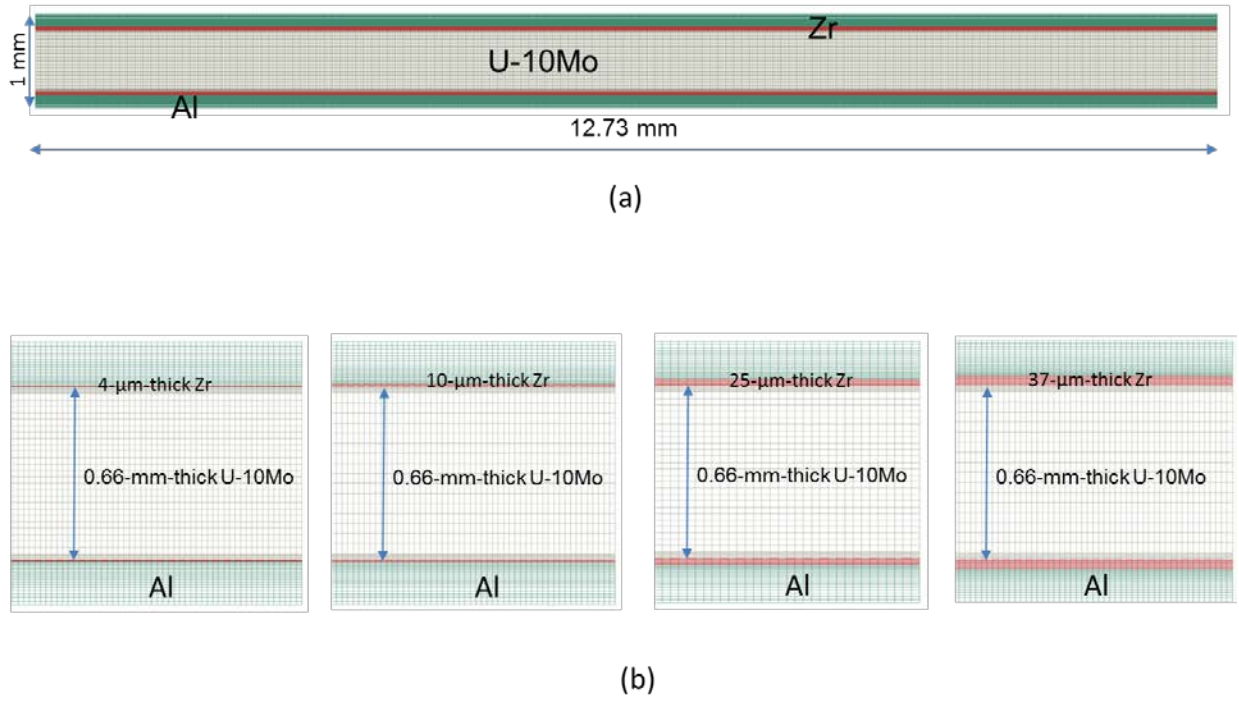

Figure 1. (a) Illustration of a Two-Dimensional FE Mesh of the Al/Zr/U-10Mo Foil with Smooth Interfaces, and (b) Snapshots Showing Detailed Meshes Containing Zr Layers of Different Thicknesses

The foil model was subjected to the boundary conditions illustrated in Figure 2. It was fixed at one end while the other end was subjected to a uniform rotation resulting in a uniform moment M (Figure 2a). The moment M was increased incrementally to a maximum value to cause a permanent curvature radius of 76.58 mm (3.015 in.) after springback (Figure 2b). Thus, the maximum value of the moment to cause the same permanent deformed shape of the foil after springback was different from one foil model to another when the thickness and mechanical properties of the Zr layer varied. The permanent curvature radius of 76.58 mm after springback was used as an analysis criterion in the sensitivity study. Considering four thickness values of the Zr layer and three mechanical behaviors of Zr resulted in 12 analysis cases with smooth interfaces.

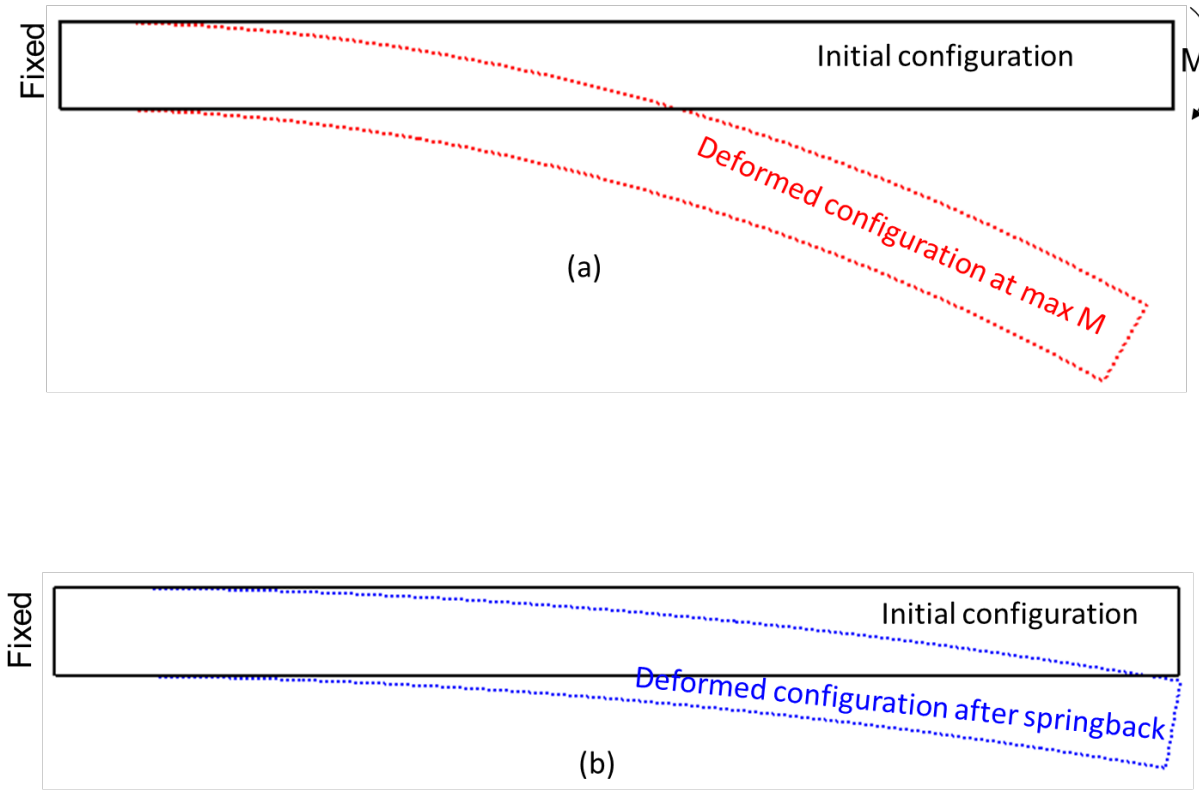

Figure 2. (a) Boundary Conditions Applied to Deform the Al/Zr/U-10Mo Foil Involving a Uniform Applied Moment to Cause (b) the Permanent Deformed Configuration after Springback Achieving a Curvature Radius of 76.58 mm (3.015 in.)

2.2 A FE Model with Rough Interfaces

A FE high-resolution mesh of an actual and typical foil cross section was created from a microstructural image using the National Institute of Standards and Technology's (NIST's) OOF2 software.[1] From this initial mesh, an ABAQUS FE model was built that includes the asperities (roughness) along the interfaces between the Zr layers with the adjacent Al and U-10Mo layers. Figure 3 presents the FE model for the whole foil and a snapshot showing high-resolution microstructural mesh details along the interfaces. This foil model has the same overall dimensions as the models without interface roughness (1 mm thick and 12.73 mm wide, Figure 1). It contains the Zr layers with locally varying thicknesses. The mean thickness of the Zr layers is about 25 microns. The FE model with interface roughness was also subjected to the boundary conditions depicted in Figure 2. It was used to investigate the effect of the interface roughness on the foil's integrity.

[1] Software developed at the National Institute of Standards and Technology.

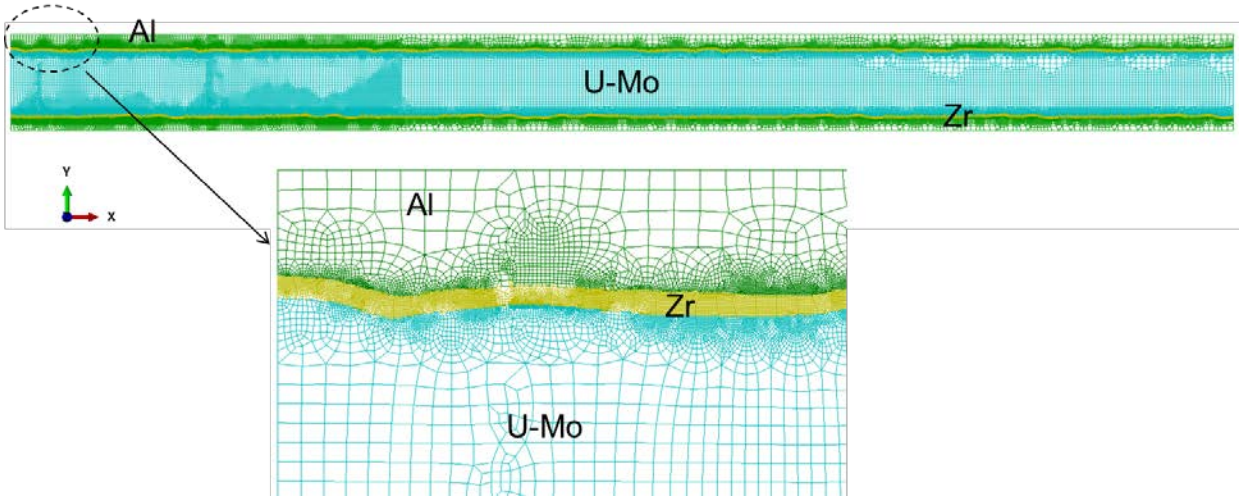

Figure 3. A High-Resolution FE Model of the Al/Zr/U-10Mo Foil with Rough Interfaces

3.0 Mechanical Properties

FE analyses of the Al/Zr/U-10Mo foil using the elastic-plastic model with isotropic hardening and isotropic ductile damage of the ABAQUS's constitutive laws library require the input data for the elastic properties (i.e., elastic modulus and Poisson's ratio), the yield stress as a function of the equivalent plastic strain, and the damage evolution behavior for each material of the foil. These data can be obtained from the material tensile uniaxial stress-strain response assuming isotropic behavior. In this work, we used the Idaho National Laboratory stress-strain data for Al-6061-HIP-L1T1 (Lloyd 2013) (Figure 4) to obtain the model parameters for the Al layers of the foil. The stress-strain response of U-10Mo was estimated based on Rest et al. (2009) and Burkes et al. (2009) (Figure 5). For Zr, we considered three types of behavior representing the pure or nearly pure Zr (named Zr(1)), low-O_2 (~30 (wt ppm)$^{1/2}$) content Zr (Zr(2)), and very high O_2 content (> 100 (wt ppm)$^{1/2}$) Zr (Zr(3)). The low and high O_2-content Zr materials correspond to two Zr named DUM926 and DUM913, for which Pacific Northwest National Laboratory's Vickers hardness data are available. Using these data, the yield stress at 0.2% equivalent plastic strain and the ultimate tensile strength were estimated using the formulas of Cahoon et al. and Tabor, respectively (Cahoon et al. 1971; Tabor 1951):

$$\sigma_y = \frac{H_V}{3}(0.1)^{m-2} \tag{1}$$

$$\sigma_u = \frac{H_V}{2.9}[1-(m-2)]\left[\frac{12.5\,(m-2)}{1-(m-2)}\right]^{m-2} \tag{2}$$

where H_v is the Vickers hardness and σ_y and σ_u denote the yield stress at 0.2% equivalent plastic strain and the ultimate tensile strength. Parameter m is the Meyer's hardness coefficient; $(m-2)$ values for some common alloys were reported in the [0.08, 0.23] range (Cahoon et al. 1971). In this work $(m-2)$ was assumed to be 0.09 for DUM926 and DUM913.

The H_v mean values for DUM926 (Zr(2)) and DUM913 (Zr(1)) are 163.3 kgf/mm^2 (1601 MPa) and 526.3 kgf/mm^2 (5161 MPa), respectively. The applications of Equations (1) and (2) produce the corresponding

values of σ_y and σ_u for Zr(2) and Zr(3) given in Table 1. The H_v data for the nearly pure Zr (Zr(1)) were not available. In this work, we assumed that Zr(1) has the lowest ultimate tensile strength equal to the yield stress at 0.2% (= 280 MPa) and the largest elongation limit (= 0.4), while Zr(3) (corresponding to DUM913) is rather brittle and possesses the highest ultimate tensile strength (1400 MPa) with a very small elongation limit (~0.02). Between these two extreme behaviors, Zr(2) (corresponding to DUM926) represents a more typical behavior with a 0.15 elongation limit and an ultimate tensile strength of about 512 MPa. These assumed Zr behaviors are depicted in Figure 6.

Table 1 presents the key mechanical properties for each foil material needed for the analyses, including the elastic properties, the yield stress at 0.2% equivalent plastic strain, the ultimate tensile strength, and the assumed elongation limits.

Table 1. Mechanical Properties of the Foil Layers for Nonlinear FE Analyses

Material	Elastic Modulus (MPa)	Poisson Ratio	Yield Stress at 0.2% (MPa)	Ultimate Tensile Strength (MPa)	Elongation Limit	Notes
Al	68,900	0.3	69.5	193	0.3	Typical Al
Zr(1)	88,000	0.34	280	280	0.4	Pure Zr
Zr(2)	88,000	0.34	434	512	0.15	Low Oxygen Zr
Zr(3)	88,000	0.34	1,400	1,400	0.02	High oxygen Zr
U-Mo	85,500	0.3	954	954	0.16	Typical U-Mo

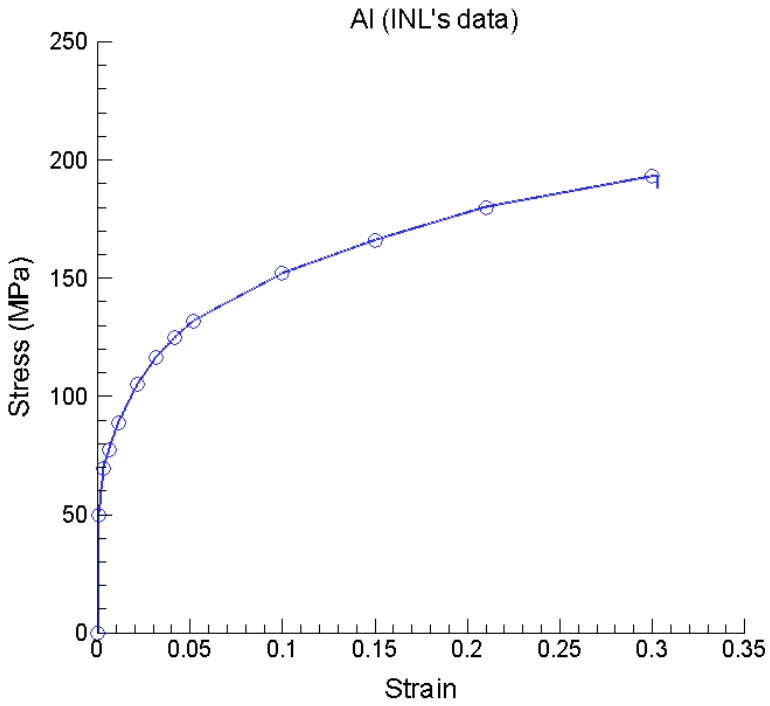

Figure 4. The True Stress-Strain Response of Al-6061-HIP-L1T1 Based on Idaho National Laboratory's Data (Lloyd 2013)

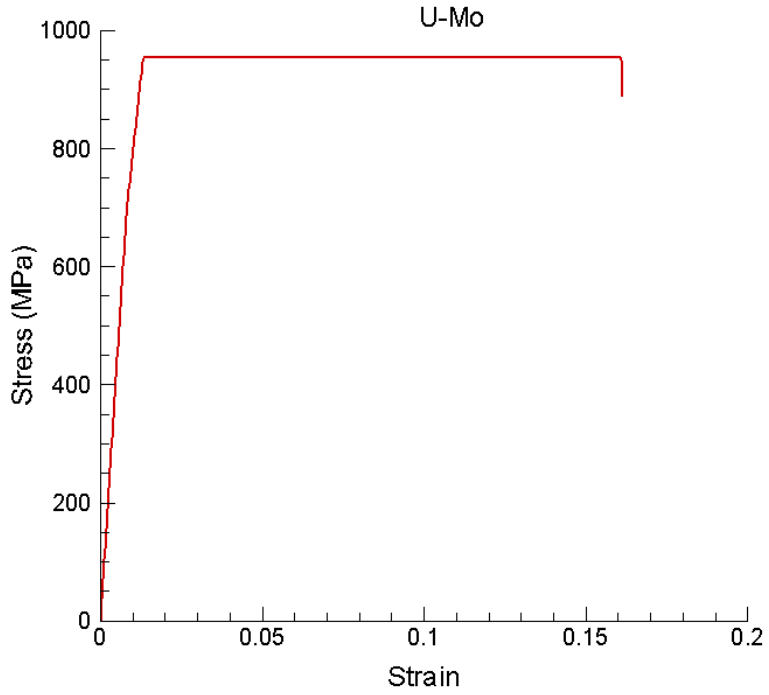

Figure 5. The Estimated Stress-Strain Response of U-10Mo Based on Rest et al. (2009) and Burkes et al. (2009)

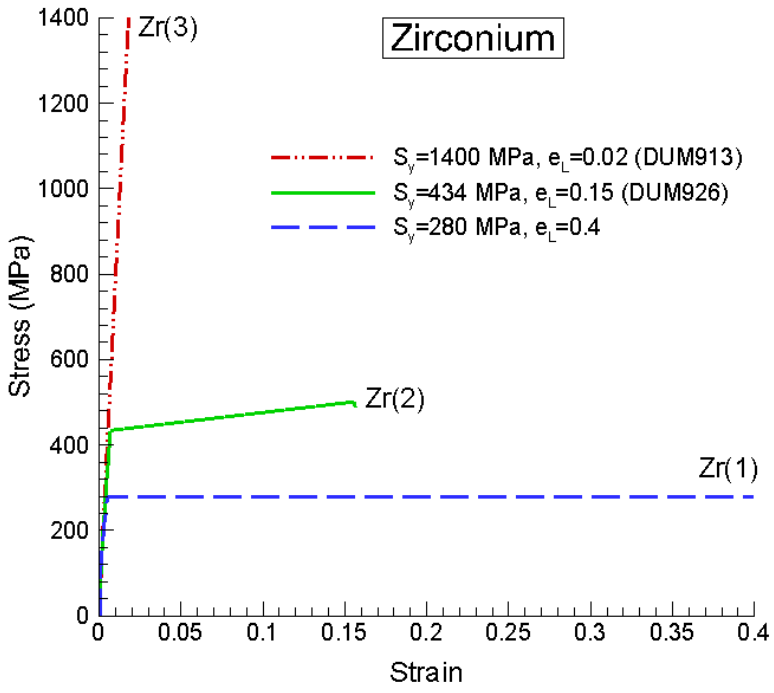

Figure 6. The Assumed Uniaxial Stress-Strain Behaviors of Zr for the Sensitivity Analysis

4.0 Results and Discussions

4.1 Effects of Zr-Layer Thickness and Mechanical Properties

This section reports the analysis results showing the effects of Zr-layer thickness (using the FE models presented in Figure 1b) and the associated mechanical properties (Table 1, Figure 4–Figure 6) on the foil responses in terms of the distributions of Von Mises equivalent stresses, equivalent plastic strains, and damage development. Detailed illustrations of the analysis results are given in this section for the foil models containing 25-micron-thick Zr layers whose stress-strain behaviors follow the curves for Zr(1), Zr(2), and Zr(3) depicted in Figure 6.

Figure 7a–Figure 7c show the contours of equivalent Von Mises stresses in these foils obtained at the maximum applied moments (before loading suppression). Similar equivalent stress distributions were found in the U-10Mo core by the analyses for Zr(1) and Zr(2). In the very narrow regions along the boundaries with the Zr layers, the U-10Mo core has flowed plastically as indicated by the equivalent stresses attaining the yield stress of U-10Mo (~954 MPa, Table 1). The Al and Zr layers also have attained stress levels exceeding the respective values at 0.2% equivalent plastic strain. These layers experienced much more significant yielding than the U-10Mo core. Very high stress levels attained in the Zr layers predicted by the analysis for Zr(3) have caused more stress concentrations along the interfaces between the Zr layers and U-10Mo core in this case.

The equivalent Von Mises stress distributions after springback are reported in Figure 8a–Figure 8c. Because the U-10Mo core was still almost elastic at the maximum moments, the unloading at the moment removal first reduced the stress levels in all the layers. However, as the accumulated elastic deformation energy continued to be released, it led to stress re-buildup in the Zr and Al layers and caused additional damage in these layers until the foil structure reached an equilibrium at the permanent deformed shape (corresponding to the curvature radius of 76.58 mm [3.015 in.] after springback). Low stress levels were found in the U-10Mo core after springback in all cases. The analysis for Zr(3) predicted a significant reduction of stress after springback (Figure 8c) due to the substantial damage that caused the Zr layers to approach failure.

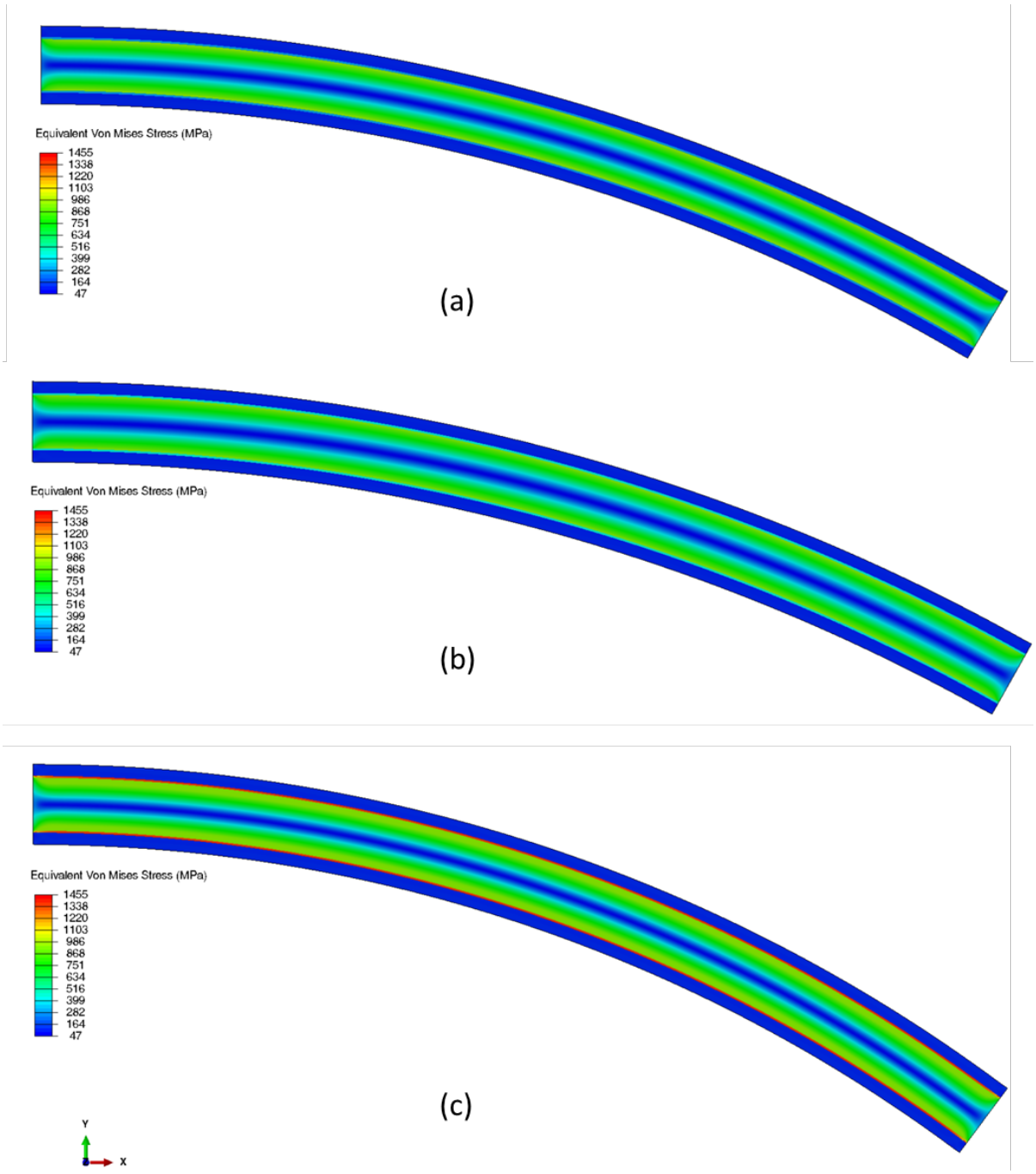

Figure 7. Contours of Von Mises Equivalent Stresses at the Maximum Applied Moment: Analysis for (a) Zr(1), (b) Zr(2), and (c) Zr(3)

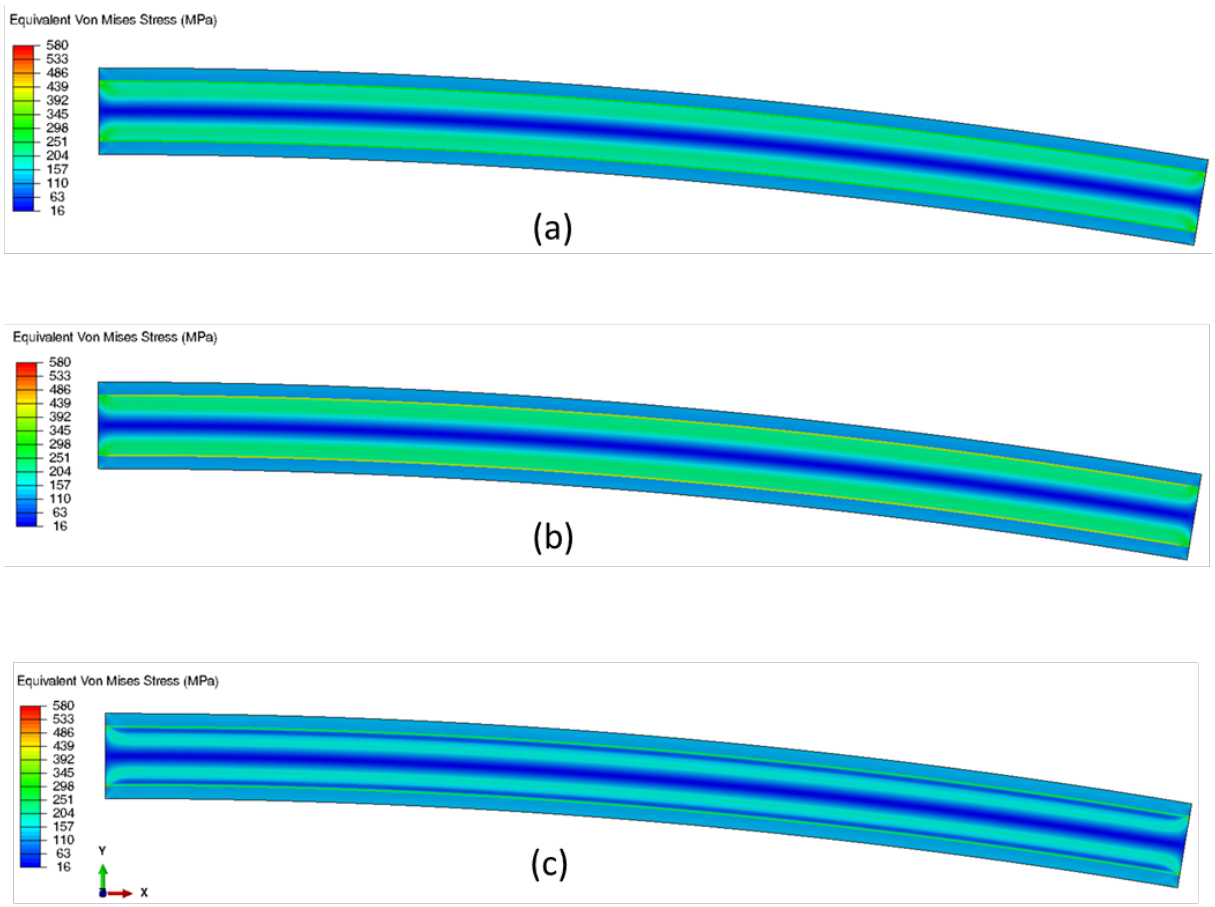

Figure 8. Contours of Von Mises Equivalent Stresses in the Permanent Deformed Configuration after Springback Achieving a Curvature Radius of 76.58 mm: Analysis for (a) Zr(1), (b) Zr(2), and (c) Zr(3)

Figure 9a–Figure 9c show the contours of equivalent plastic strains in the foils obtained at the maximum applied moments. Consistent with the equivalent stress distributions, the Al layers experienced the highest plastic deformation although the Zr layers also deformed plastically. The analysis for Zr(3) predicted even more plastic deformation for the Al layers. This is obvious because the Zr(3) material exhibited very little deformation (Figure 6), and plastic strains then accumulated more in the Al layers that had a much lower yield stress. The U-Mo core still remained elastic at the maximum applied moments except for the regions along the interfaces with the Zr layer that underwent plastic deformation to a very little extent. The equivalent plastic strain distributions after springback are presented in Figure 10a–Figure 10c. As mentioned earlier, after an initial unloading, the elastic deformation energy released from the U-10Mo core caused additional plastic deformation in the Al and Zr layers, leading the foils to a permanent shape after springback.

The damage distributions (contours of the damage indicator) in the foils predicted at the maximum applied moments and after springback are shown in Figure 11a–Figure 11c and Figure 12a–Figure 12c, respectively. The damage indicator can vary between 0 and 1. The zero value indicates virgin undamaged material, and the unity value theoretically indicates a totally damaged material corresponding to material failure or fracture. In a real physical situation, an element of material could break before the damage indicator reaches the value of 1. Therefore, depending on the brittle or ductile behavior of fracture, the critical value of the damage indicator at fracture initiation can be significantly less than or close to 1. At the maximum moments, negligible damage (damage indicator < 0.08) was predicted in all the layers for

the analyses using materials Zr(1) or Zr(2). However, the analysis for Zr(3) predicted substantial damage (damage indicator in the [0.9, 1] range) indicating that Zr layers fracture. During springback, the release of the elastic deformation energy accumulated in the U-10Mo core produced even more damage in the Al and Zr layers (Figure 12a-Figure 12c).

The contours of governing variables illustrated in Figure 7–Figure 12 show that all the through-thickness distributions are similar from one location to another except for the foil extremity regions. Therefore, it is meaningful to examine the through-thickness distributions of these variables at a given location away from the extremities. In the following narrative, we illustrate the through-thickness results at the foil mid-section location for all 12 cases with smooth interfaces.

Figure 13a–Figure 13c show the through-thickness distributions of the equivalent Von Mises stresses at the maximum applied moments for all the cases obtained from the analyses of Zr(1), Zr(2), and Zr(3), respectively. Similar equivalent stress distributions were found in the U-10Mo core for Zr(1) and Zr(2). In the locations close to the Zr layers, the U-10Mo core underwent plastic deformation in all the cases, as indicated by the equivalent stresses attaining the yield stress of U-10Mo (~954 MPa, Table 1). The locations in the Al and Zr layers also have attained stress levels exceeding the respective values at 0.2% equivalent plastic strain. Very high stress levels attained in the Zr layers were predicted for Zr(3) for all cases. For a given Zr material, the Zr-layer thickness was found to have little effect.

The through-thickness equivalent Von Mises stress distributions after springback obtained from the analyses for Zr(1), Zr(2), and Zr(3) are depicted in Figure 14a–Figure 14c, respectively. As explained previously, unloading right after the bending moment removal reduced the stress levels in all the layers. However, as the accumulated elastic deformation energy continued to be released, it led to stress buildup in the Zr and Al layers which caused additional damage in these layers until the foil structure reached equilibrium at the permanent deformed shape. Low to moderate equivalent stress levels were found in the U-10Mo core after springback for all cases. However, significantly higher values equal to or exceeding the corresponding yield stress were found in the Zr layers for Zr(1) (Figure 14a) and Zr(2) (Figure 14b). The analysis for Zr(3) predicted a significant reduction of stress after springback (Figure 14c) due to substantial damage causing fracture of the Zr layers. Compared to the equivalent stress distributions at the maximum applied moments (Figure 13a–Figure 13c), the residual equivalent stress contours after springback reveal a more significant effect of the Zr-layer thickness, in particular, as predicted for Zr(1) and Zr(2). Smaller residual stresses occur in the locations of the U-10Mo core adjacent to the Zr layers and the stresses are reduced as the Zr thickness is reduced, as expected.

The through-thickness bending stresses at the maximum applied moments reported in Figure 15a and Figure 15b for Zr(1) and Zr(2) show the highest stress magnitudes (tensile or compressive) occurring in the U-10Mo core adjacent to the Zr layers. The analysis for Zr(3) predicted the highest bending stress values in the Zr layers (Figure 15c). As predicted for the equivalent stress distributions, little effect of the Zr-layer thickness on the bending stresses was also found at the maximum applied moments. Figure 16a–Figure 16c present the through-thickness bending stresses after springback. Moderate residual stress values were found in the U-10Mo core locations near the Zr layers. The effect of the Zr-layer thickness is more significant after springback than at the maximum applied moments. The analyses for Zr(1) and Zr(2) show that the thicker the Zr layer the larger are the residual bending stresses in the U-10Mo core near the Zr layers. The analysis for Zr(3) shows a significant reduction of bending stresses after springback because of stress reduction in the Zr layer approaching failure.

Figure 17a–Figure 17c show the through-thickness distributions of the equivalent plastic strains obtained at the maximum applied moments. Consistent with the equivalent stress distributions, locations in the Al layers experienced the most plastic deformation, although the locations in the Zr layers also deformed plastically. As explained previously, the analysis for Zr(3) predicted more plastic deformation for the Al

layers (more than 2%) because Zr(3) exhibits very little deformation. The U-10Mo core still remained elastic at the maximum applied moments except near the interfaces with the Zr layer that underwent plastic deformation—less than ~0.02% predicted by the analyses for Zr(1) and Zr(2), and less than 0.06% predicted for Zr(3). As found for this stress distribution, the effect of the Zr-layer thickness on the equivalent plastic strain distribution is not significant at the maximum applied moments. The equivalent plastic strain distributions after springback are presented in Figure 18a–Figure 18c. As explained earlier, after an initial unloading, the elastic deformation energy released from the U-10Mo core caused additional plastic deformation of the Al and Zr layers, as predicted by the analyses for Zr(1) (Figure 18a) and Zr(2) (Figure 18b). The analysis for Zr(3) predicted more plastic strains accumulated in the Al layers after springback (Figure 18c), because the Zr layers that exhibited very little deformations suffered from excessive damage. For the same reason, higher plastic strains were predicted to accumulate in the U-10Mo core near the Zr layers for Zr(3).

The through-thickness damage distributions predicted at the maximum applied moments and after springback are shown in Figure 19a–Figure 19c and Figure 20a–Figure 20c, respectively. At the maximum moments, negligible damage (damage indicator < 0.08) was predicted in all the layers for Zr(1) or Zr(2). However, the analysis for Zr(3) predicted substantial damage (damage indicator in the [0.8, 1] range for all the Zr thicknesses considered) leading the Zr layers to fracture or approach fracture. During springback, the release of the elastic deformation energy accumulated in the U-10Mo core produced more damage in the Al and Zr layers (Figure 20a–Figure 20c).

Table 2 provides a summary of the key information about the Al/Zr/U-10Mo foil model features and the corresponding maximum loading levels, as well as our findings about foil integrity based on damage predictions.

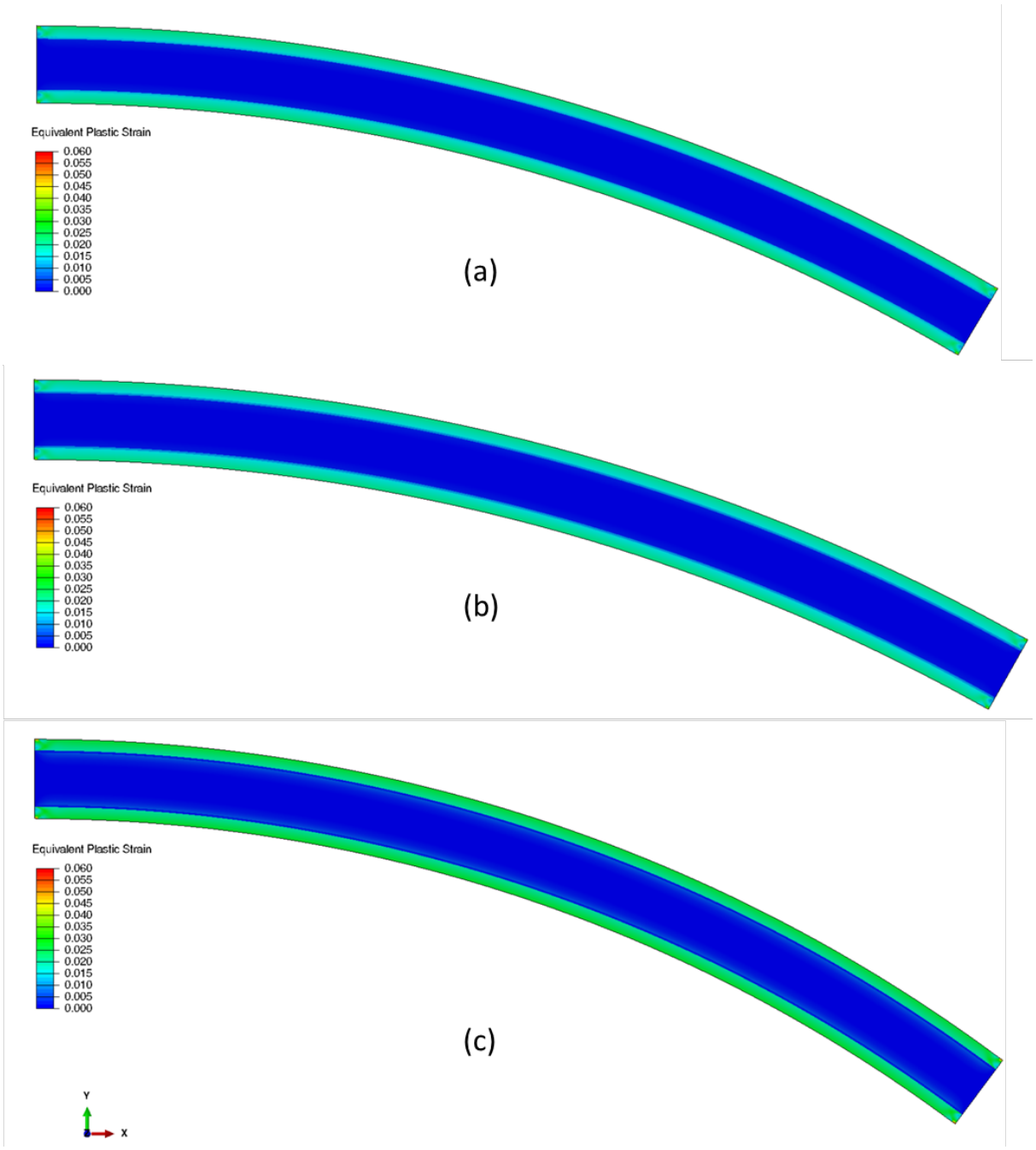

Figure 9. Contours of Equivalent Plastic Strains at the Maximum Applied Moments: Analysis for (a) Zr(1), (b) Zr(2), and (c) Zr(3)

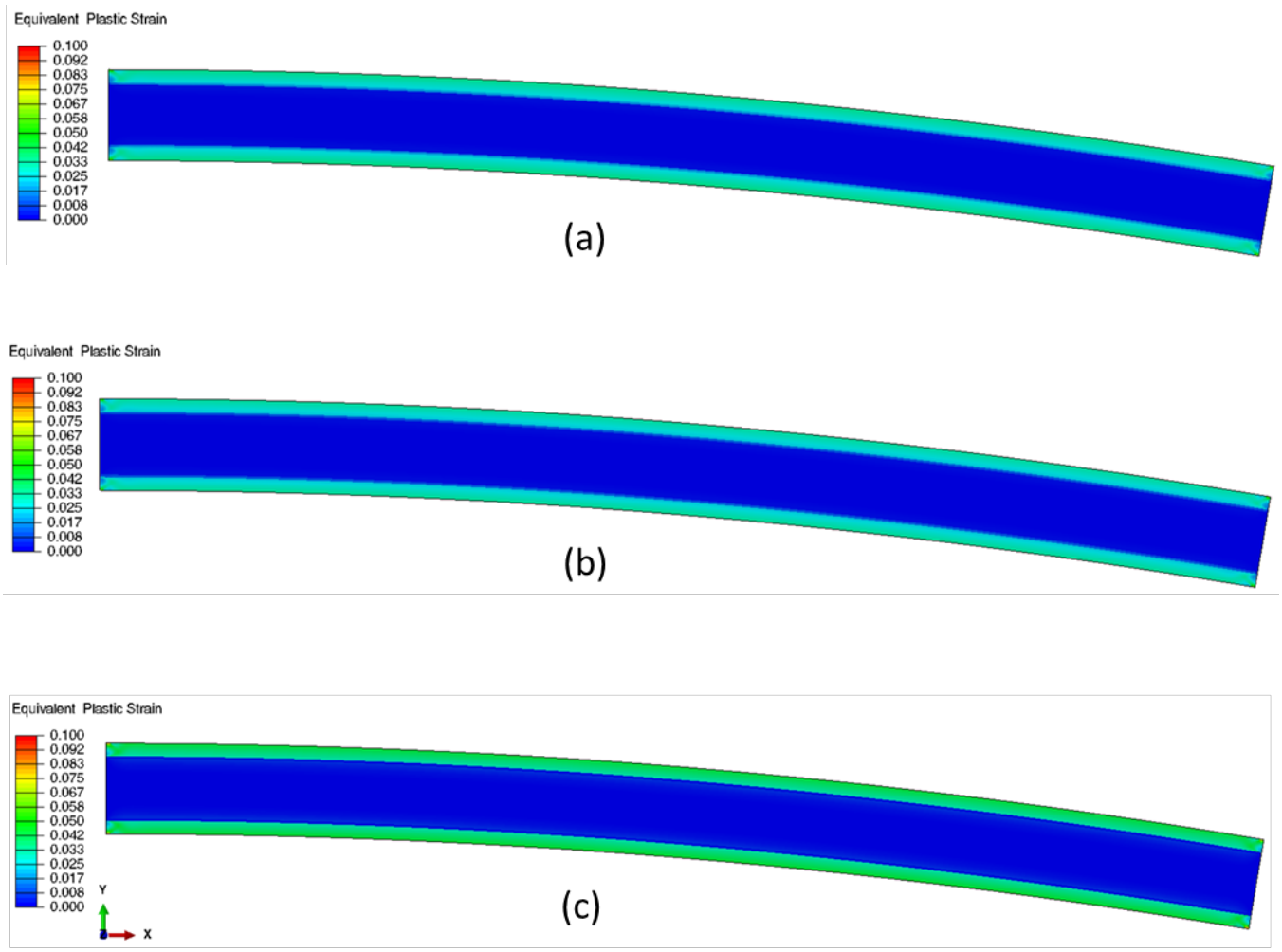

Figure 10. Contours of Equivalent Plastic Strains in the Permanent Deformed Configuration after Springback Achieving a Curvature Radius of 76.58 mm: Analysis for (a) Zr(1), (b) Zr(2), and (c) Zr(3)

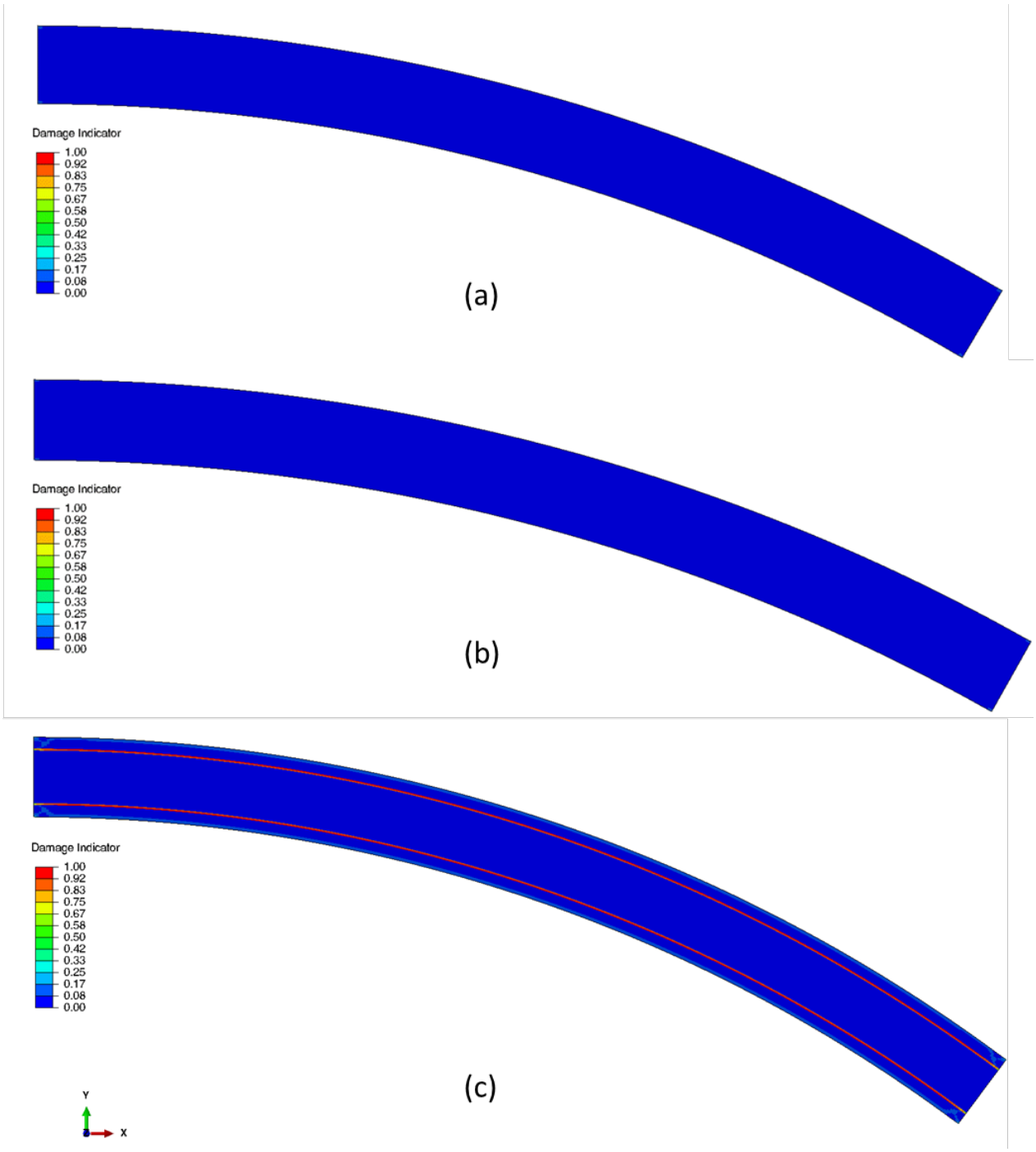

Figure 11. Damage Distributions at the Maximum Applied Moments: Analysis for (a) Zr(1), (b) Zr(2), and (c) Zr(3)

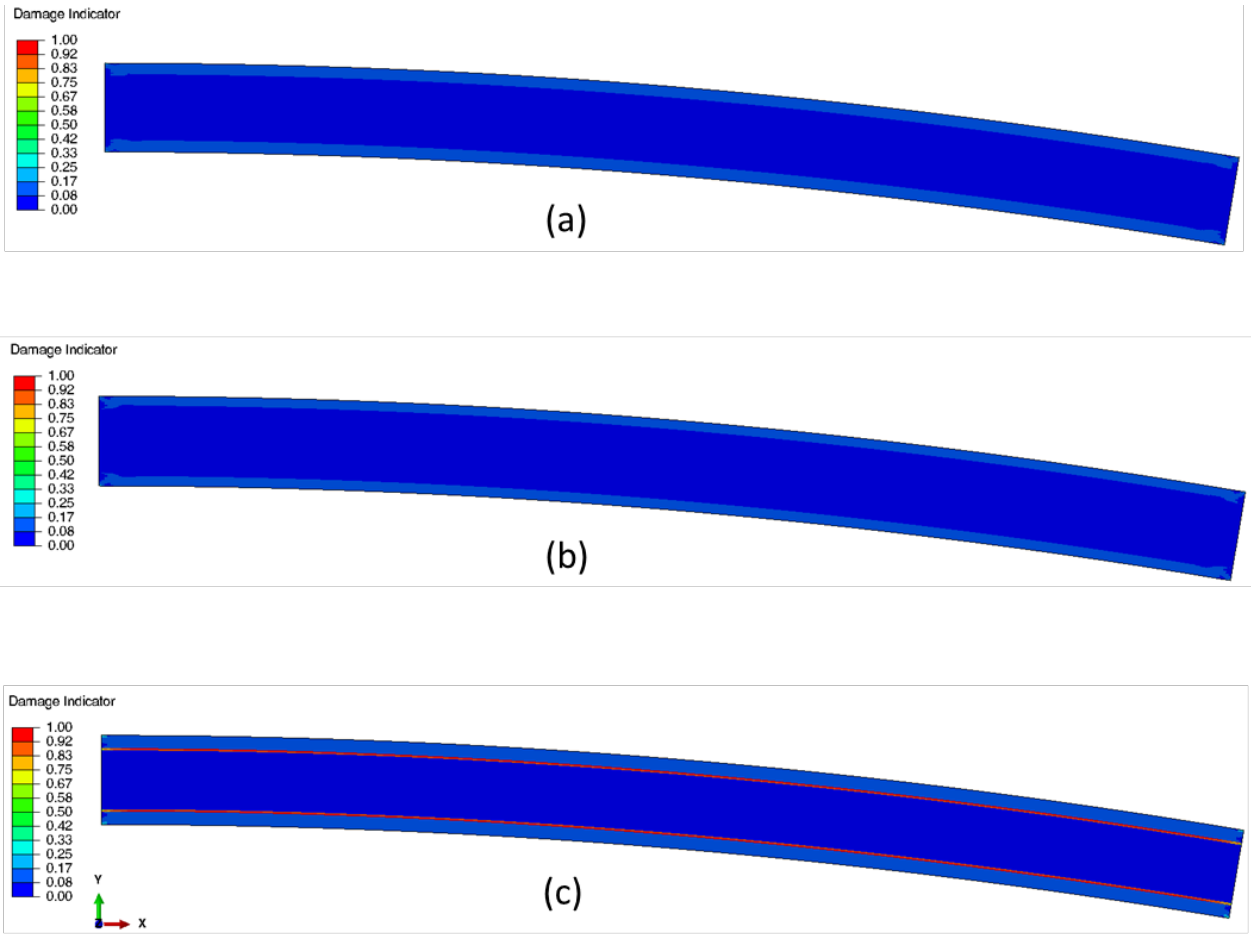

Figure 12. Damage Distributions in the Permanent Deformed Configuration after Springback Achieving a Curvature Radius of 76.58 mm: Analysis for (a) Zr(1), (b) Zr(2), and (c) Zr(3)

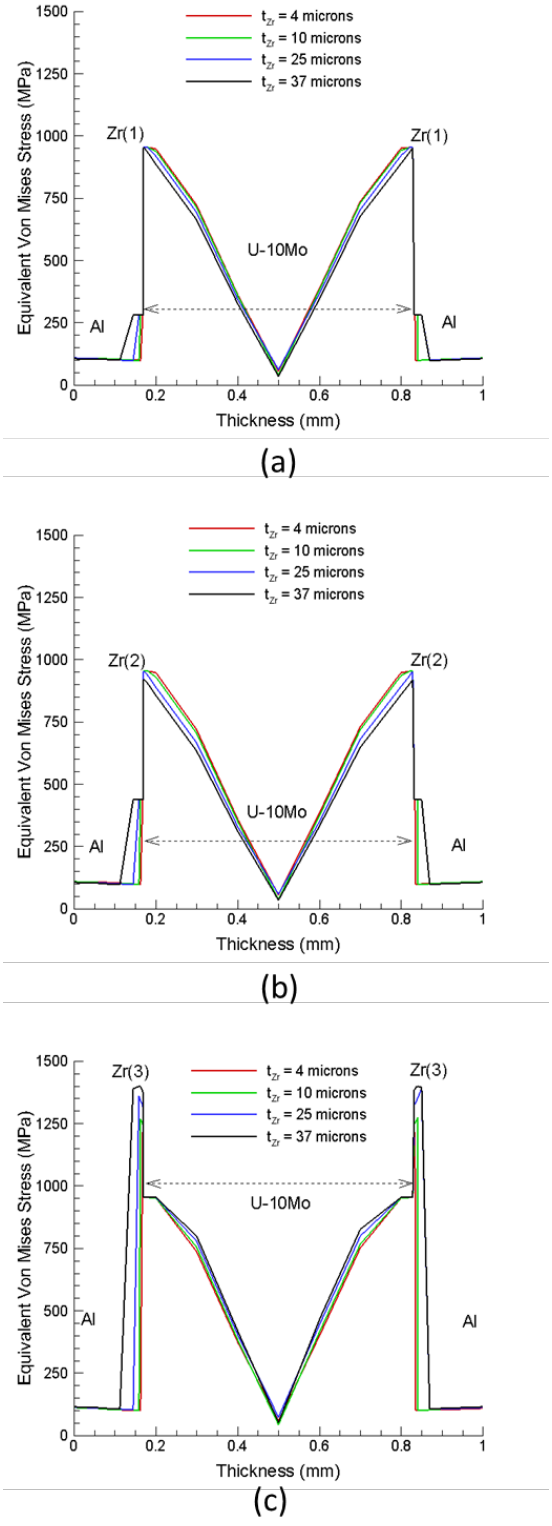

Figure 13. Through-Thickness Von Mises Equivalent Stress Distributions at the Maximum Applied Moments: Analysis for (a) Zr(1), (b) Zr(2), and (c) Zr(3)

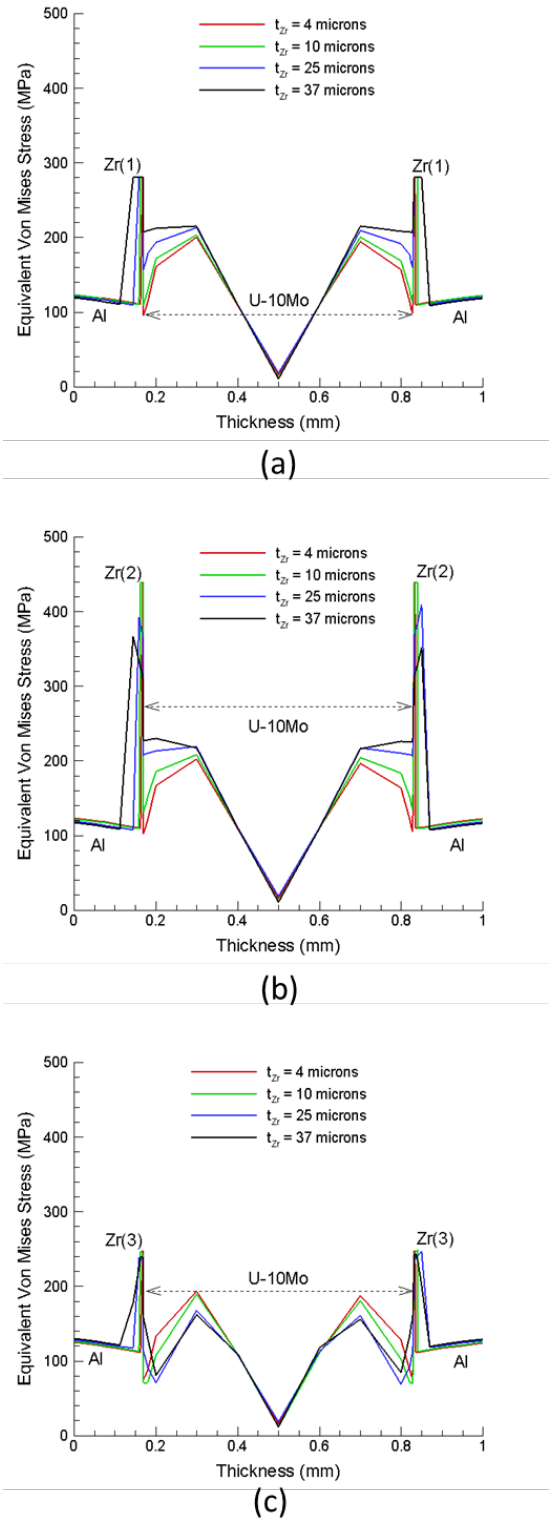

Figure 14. Through-Thickness Von Mises Equivalent Stress Distributions after Springback: Analysis for (a) Zr(1), (b) Zr(2), and (c) Zr(3)

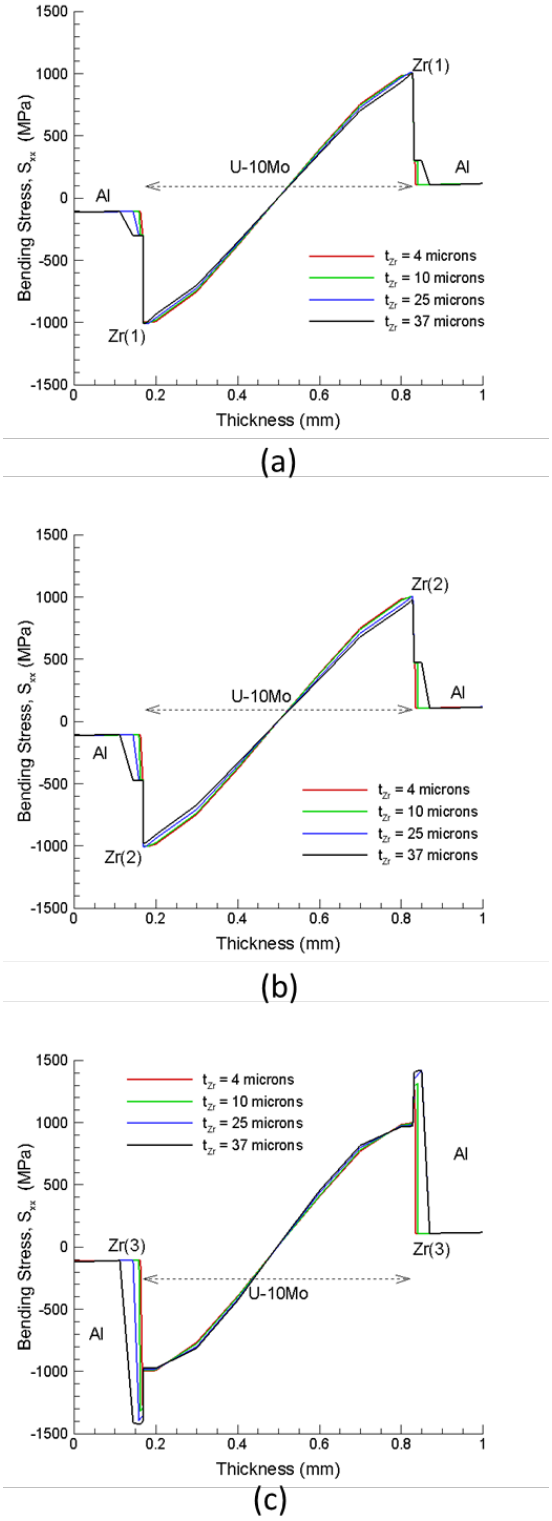

Figure 15. Through-Thickness Bending Stress Distributions at the Maximum Applied Moments: Analysis for (a) Zr(1), (b) Zr(2), and (c) Zr(3)

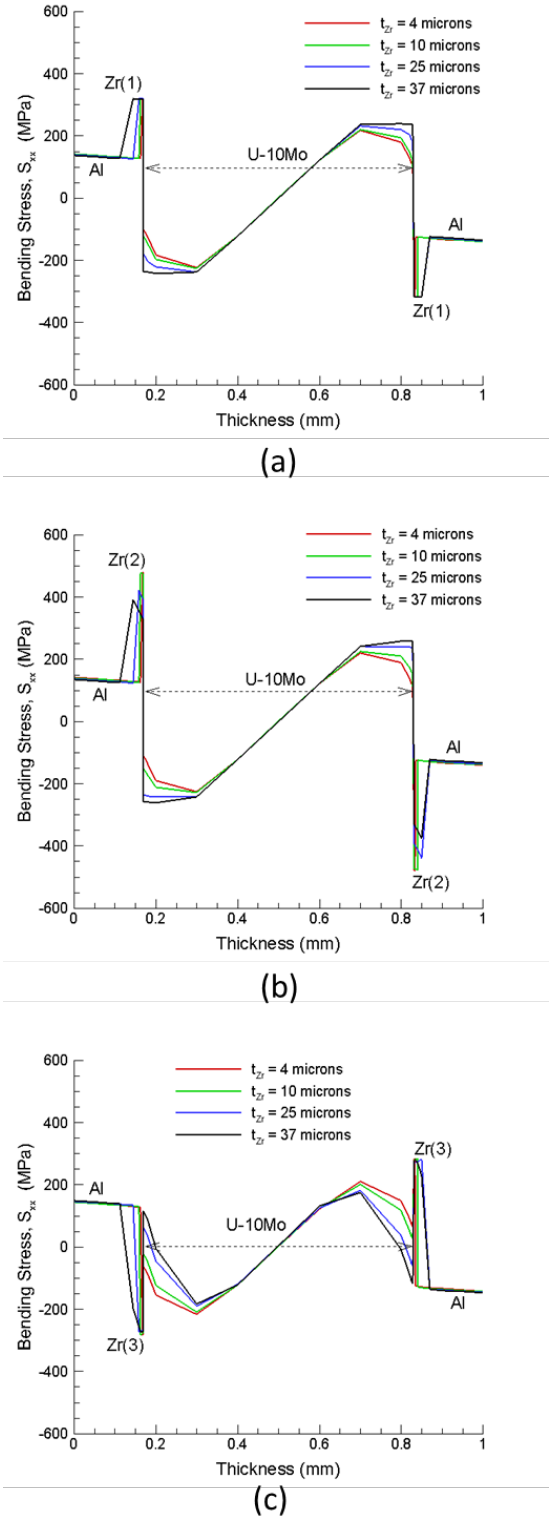

Figure 16. Through-Thickness Bending Stress Distributions after Springback: Analysis for (a) Zr(1), (b) Zr(2), and (c) Zr(3)

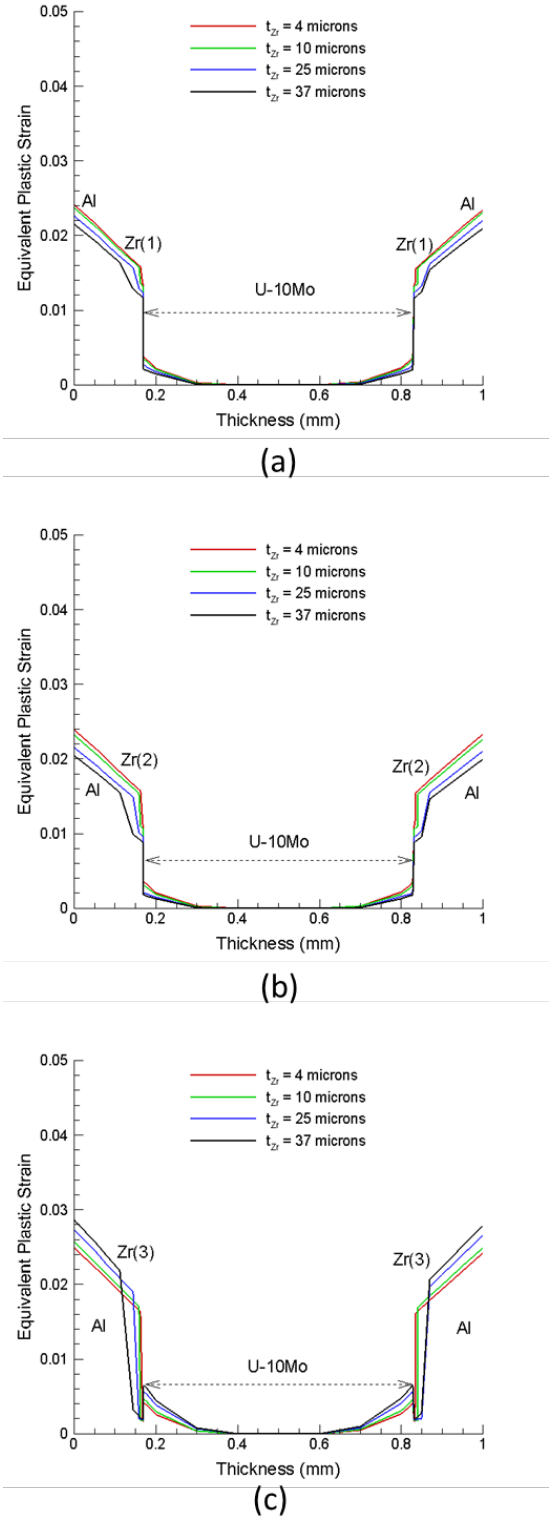

Figure 17. Through-Thickness Equivalent Plastic Strain Distributions at the Maximum Applied Moments: Analysis for (a) Zr(1), (b) Zr(2), and (c) Zr(3)

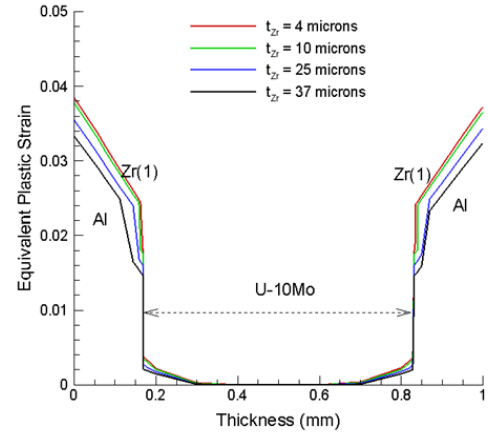

(a)

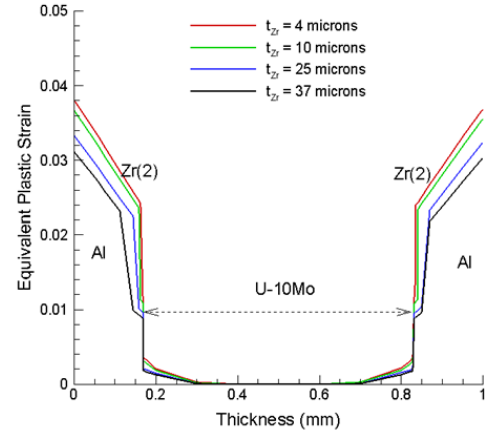

(b)

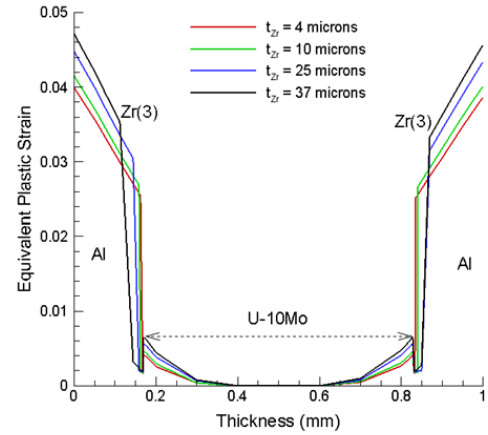

(c)

Figure 18. Through-Thickness Equivalent Plastic Strain Distributions after Springback: Analysis for (a) Zr(1), (b) Zr(2), and (c) Zr(3)

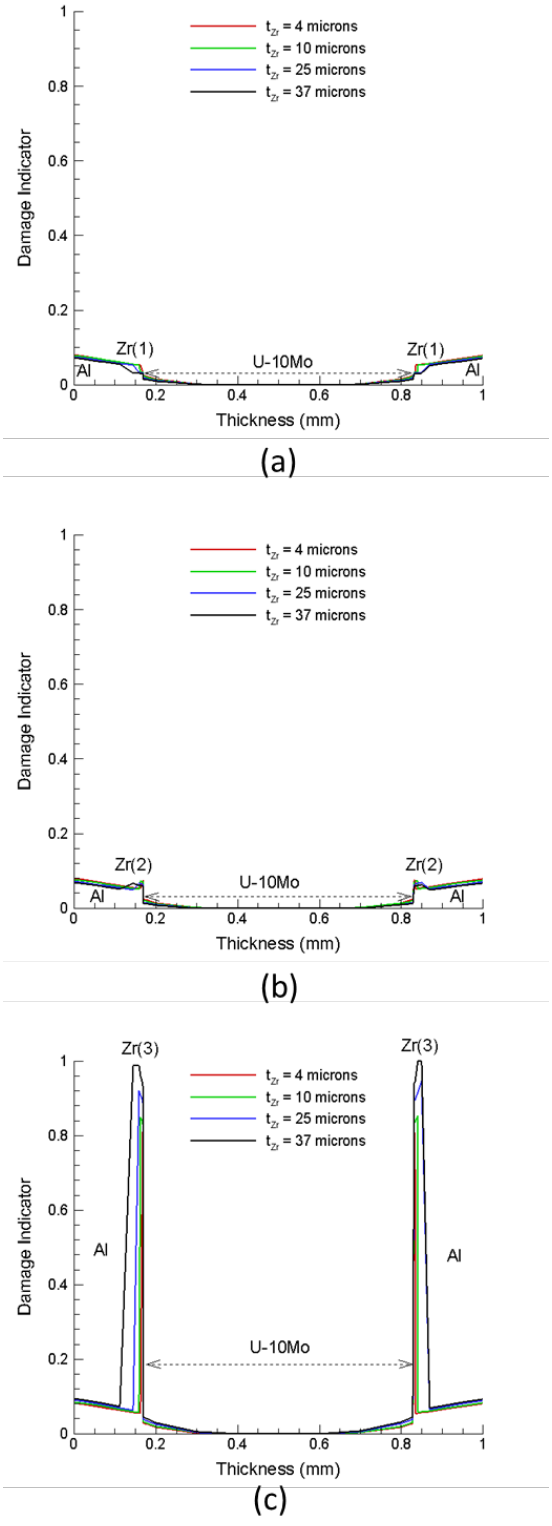

Figure 19. Through-Thickness Damage Indicator Distributions at the Maximum Applied Moments: Analysis for (a) Zr(1), (b) Zr(2), and (c) Zr(3)

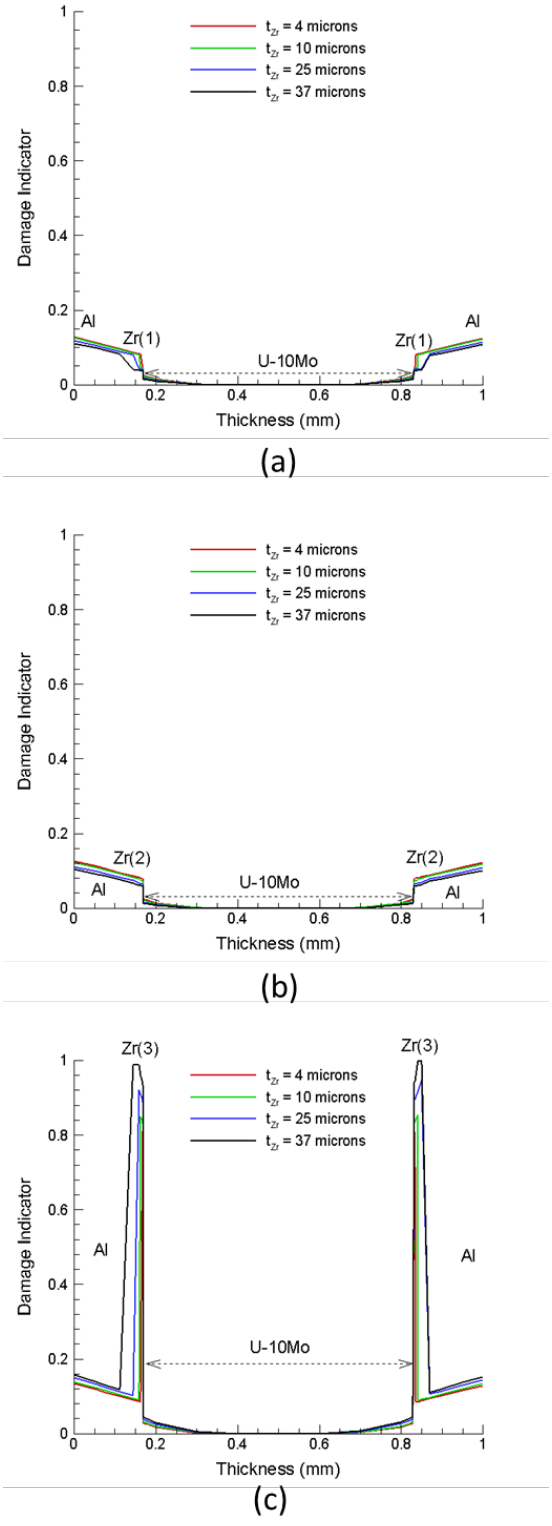

Figure 20. Through-Thickness Damage Indicator Distributions after Springback: Analysis for (a) Zr(1), (b) Zr(2), and (c) Zr(3)

Table 2. Summary of Al/Zr/U-10Mo Foil Model Features, Maximum Loading Levels, and Damage Predictions

U-Mo/Zr Interface Defects	U-Mo/Zr Interface Smoothness	Uniform Zr Thickness (μm)	O_2 Content	Cracks from Bending	Max. Moment per mm (N)
No	Yes	4	Pure Zr	No, but minor damage	108.7
No	Yes	4	Low	No, but minor damage	108.9
No	Yes	4	Very high	Yes	113.3
No	Yes	10	Pure Zr	No, but minor damage	108.6
No	Yes	10	Low	No, but minor damage	108.7
No	Yes	10	Very high	Yes	120.4
No	Yes	25	Pure Zr	No, but minor damage	108.1
No	Yes	25	Low	No, but minor damage	108.3
No	Yes	25	Very high	Yes	139.2
No	Yes	37	Pure Zr	No, but minor damage	106.8
No	Yes	37	Low	No, but minor damage	108.1
No	Yes	37	Very high	Yes	154.5

4.2 Effect of Interface Roughness

Section 2.2 presents an Al/Zr/U-10Mo foil model with interface roughness (asperities) developed during this study to evaluate the effect of the interface roughness on foil integrity (Figure 3). The foil model with interface roughness was subjected to the boundary conditions depicted in Figure 2, under which a uniform bending moment was applied at one end of the foil while the other end was fixed. In this section, we examine the interface roughness effect by comparing the analysis results for the foil with interface roughness to those of the foil model with smooth interfaces discussed in Section 4.1. The Zr(2) material was assumed for all the Zr layers. The permanent curvature radius of 76.58 mm after springback was used as an analysis criterion in this study.

Figure 21a and Figure 21b present the contours of equivalent Von Mises stresses at the maximum applied moment obtained from the models with and without interface roughness. The model with smooth interfaces predicted similar through-thickness distributions from one section to another (Figure 21a), and stress concentrations were found to be similarly distributed along the interfaces between the Zr layers and U-10Mo core. However, the model with interface roughness predicted non-uniform stress distributions caused by the presence of asperities. Depending on the asperity geometry, stress concentrations were found along the interfaces between the U-10Mo core and the Zr layer (Figure 21b). The contours of equivalent Von Mises stresses after springback are given in Figure 22a–Figure 22b, which clearly show the interface roughness effect on the residual stress distribution. Compared to the solution by the model with smooth interfaces (Figure 23a), the residual equivalent stress distribution predicted by the model with interface roughness exhibits significant stress concentrations at the asperities along the interfaces between the U-10Mo core and the Zr layers. Some stress concentrations induced damage inside the U-10Mo core.

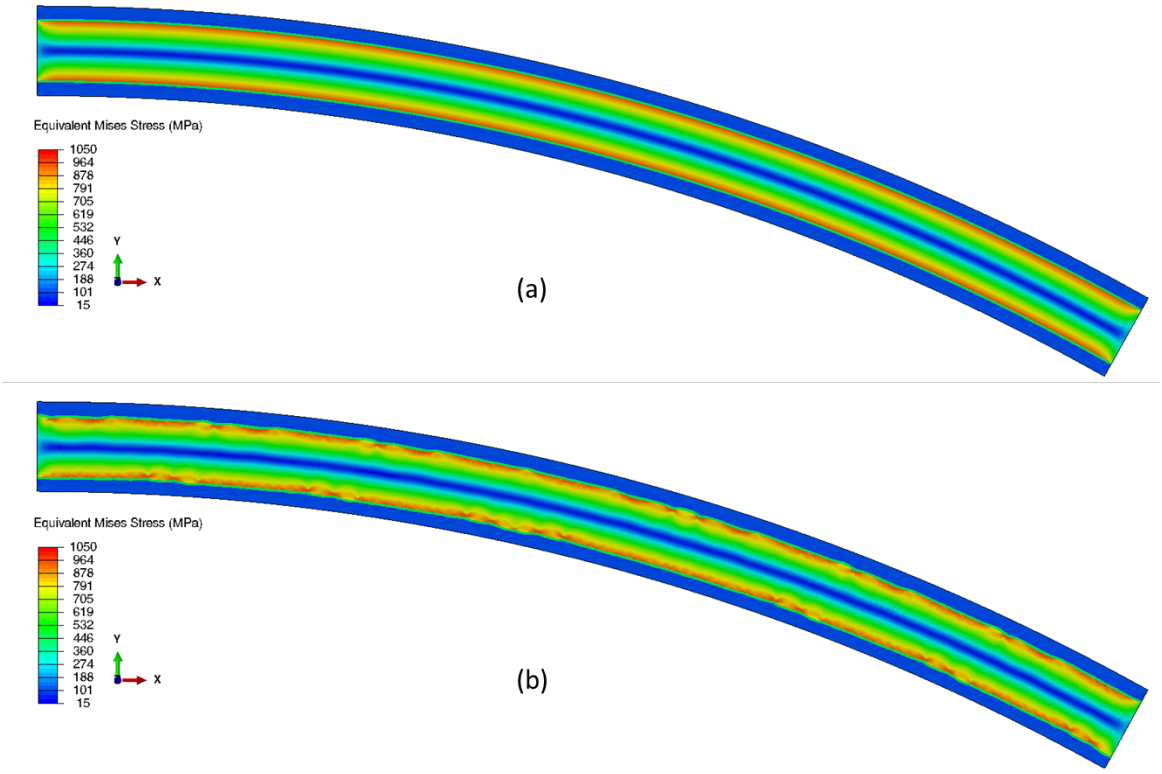

Figure 21. Contours of Von Mises Equivalent Stresses at the Maximum Applied Moment: Results from the Models with Smooth Interfaces (a) and with Interface Roughness (b)

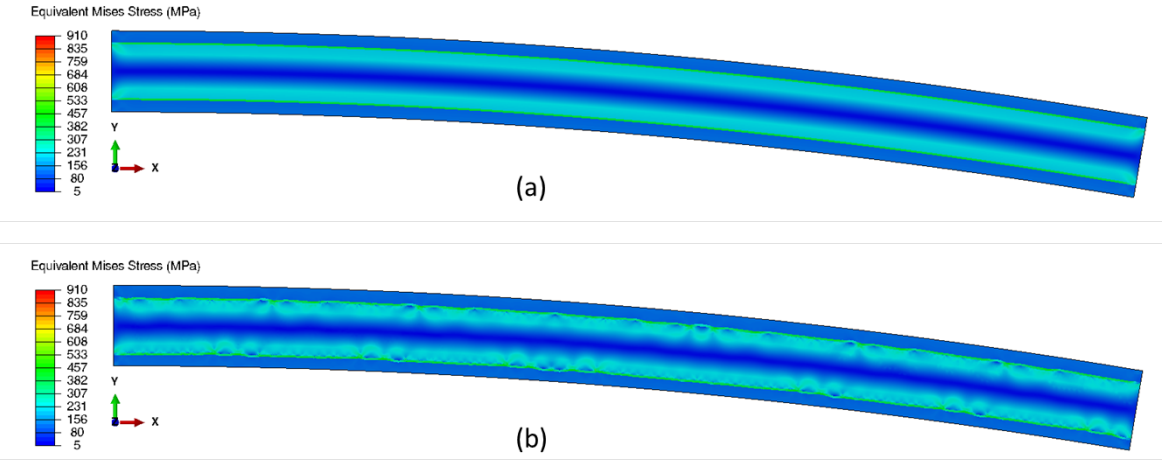

Figure 22. Contours of Von Mises Equivalent Stresses after Springback: Results from the Models with Smooth Interfaces (a) and with Interface Roughness (b)

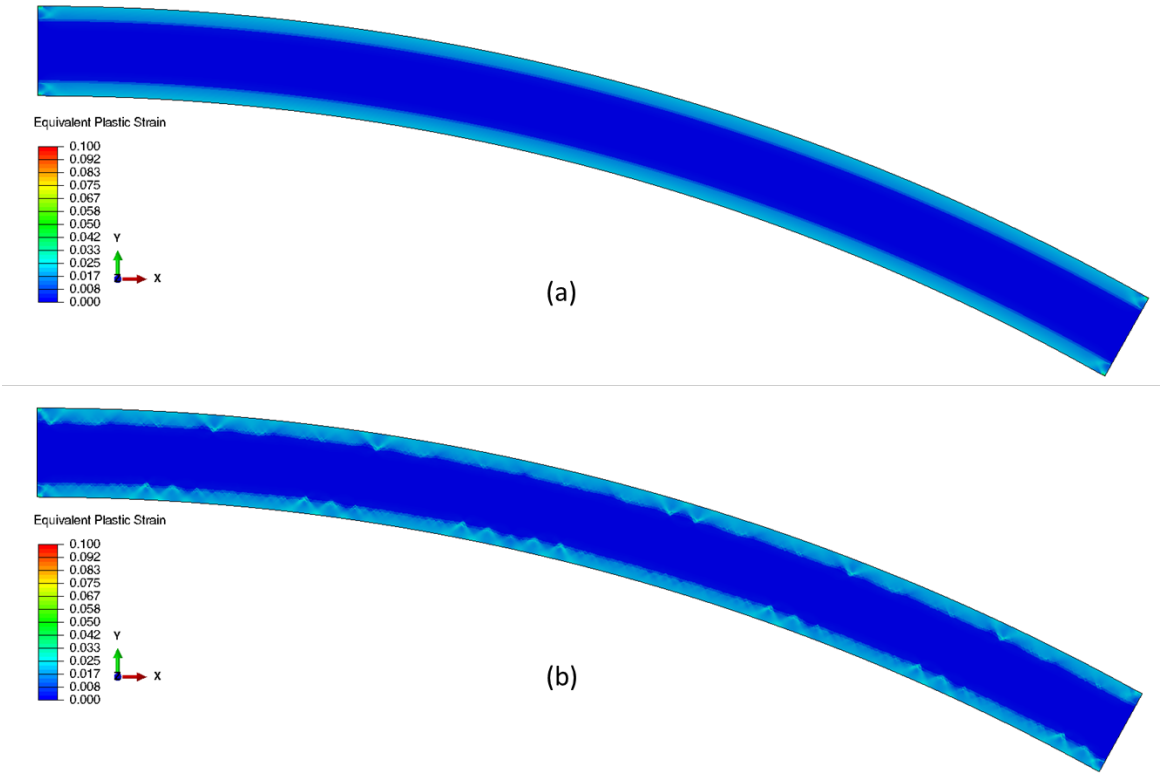

Figure 23. Contours of Equivalent Plastic Strains at the Maximum Applied Moment: Results from the Models with Smooth Interfaces (a) and with Interface Roughness (b)

The contours of equivalent plastic strains at the maximum applied moment are depicted in Figure 23a–Figure 23b. Both models predicted more plastic deformation in the Al layers, but the model with interface roughness predicted significant plastic strain concentrations at the asperities along the interfaces, as is clearly shown in Figure 23b. As explained earlier, during springback, the elastic deformation energy released from the U-10Mo core caused additional plastic deformation to the Al and Zr layers until the foil reached equilibrium after springback (Figure 24a–Figure 24b). The model without interface roughness predicted quite uniform plastic strain distributions in the Al and Zr layers (Figure 24a) while the model with interface roughness predicted plastic strain concentrations at the asperities that induced damage not only in the Al and Zr layers but also in the U-10Mo core to some extent (Figure 24b).

Figure 25a–Figure 25b and Figure 26a–Figure 26b report the damage distributions in the foil models at the maximum applied moment and after springback, respectively. The model with smooth interfaces predicted negligible damage in the Zr and Al layers, and practically no damage at all in the U-10Mo core (Figure 25a and Figure 26a). However, the model with interface roughness predicted damage concentrations at the asperities in the Zr layers and along the interfaces between the Zr layers and other layers (Figure 25b and Figure 26b). Damage accumulations further developed during springback (Figure 26b) upon the release of elastic deformation energy from the U-10Mo core caused further damage to the Zr and Al layers.

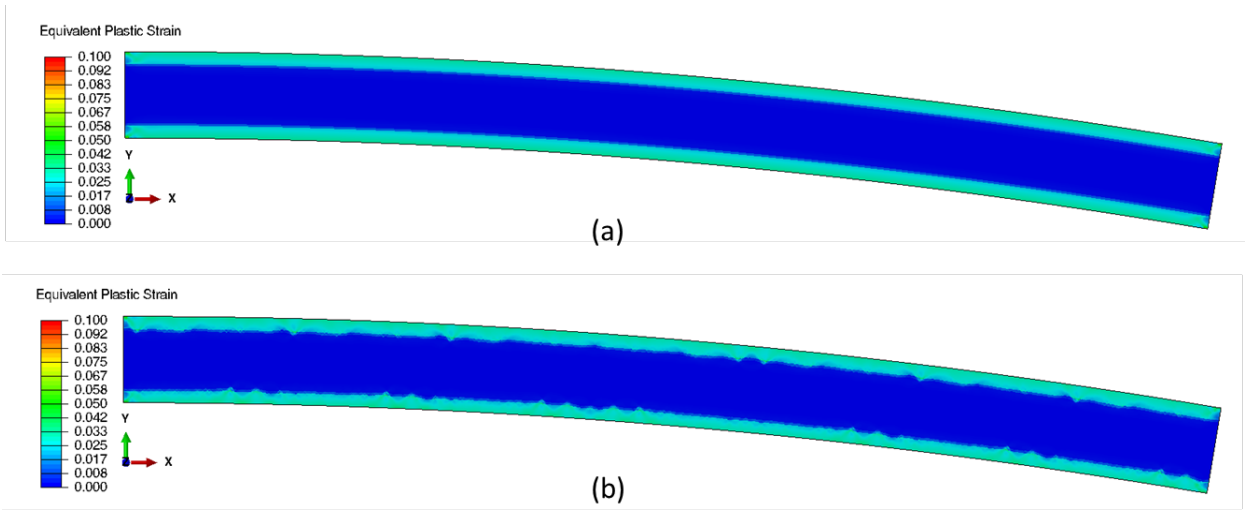

Figure 24. Contours of Equivalent Plastic Strains after Springback: Results from the Models with Smooth Interfaces (a) and with Interface Roughness (b)

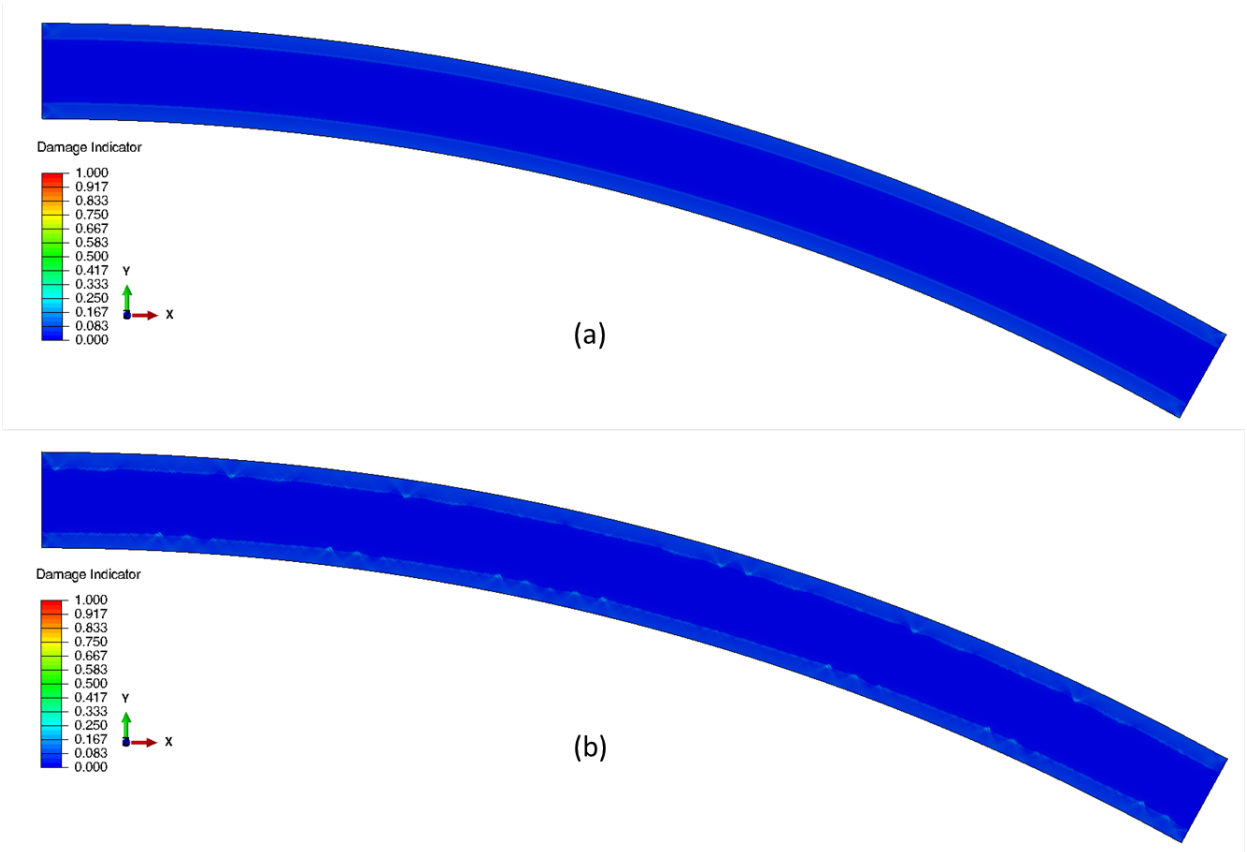

Figure 25. Damage Distributions at the Maximum Applied Moment: Results from the Models with Smooth Interfaces (a) and with Interface Roughness (b)

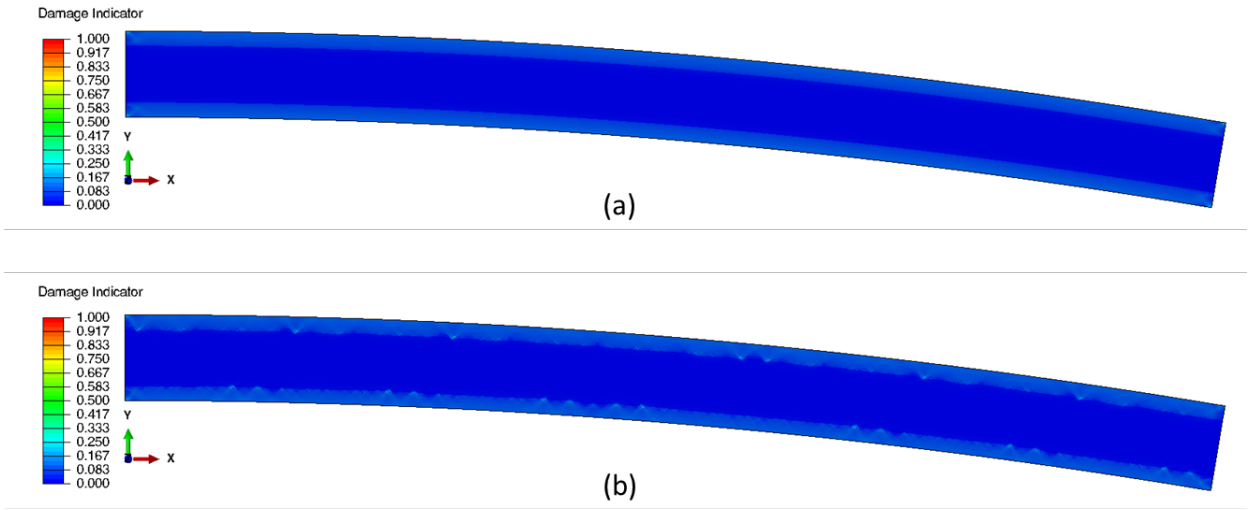

Figure 26. Damage Distributions after Springback: Results from the Models with Smooth Interfaces (a) and with Interface Roughness (b)

The analysis for the foil model with interface roughness revealed that the asperities along the interfaces between the Zr and adjacent layers were the sites of stresses, plastic strains, and damage concentrations. Damage accumulations at and near the asperities could develop into microcracks propagating in the U-10Mo core if the foil was subjected to critical loadings in practice. To further examine the effect of interface roughness on foil integrity, we considered the same foil model with interface roughness and applied the "cantilever beam" loading configuration to this model, as depicted in Figure 27. The foil section was fixed at one end, while an increasing deflection was applied at the other end.

Figure 28a–Figure 28c and Figure 29a–Figure 29c show the damage distributions around the clamped extremity of the foil at 4.5 mm and 5.5 mm applied deflections, respectively. The present analyses used materials Zr(1), Zr(2), and Zr(3) (see Figure 6) for the Zr layers. At 4.5 mm deflection, significant damage was already found in the U-10Mo core. Figure 28a–Figure 28c clearly show concentrated damages at and around some asperities, and these damage accumulations tend to further develop in the U-10Mo core. The analysis for Zr(3) predicted important damage approaching fracture for the Zr layers. A macroscopic crack propagating into the U-10Mo core is clearly seen in Figure 28c. At 5.5 mm applied deflections, many cracks are predicted to occur from the asperities and propagate more deeply into the U-10Mo core, as shown in Figure 29a–Figure 29c.

The analyses using the model with rough interfaces indicate that, depending on the loading mode and intensity, stress and damage concentrations at the asperities along the interfaces could develop in cracks propagating inside the U-10Mo core. This problem is further illustrated in Figure 30a–Figure 30b, which show the damage distributions in the clamped regions predicted by the models with smooth interfaces (Figure 30a) and rough interfaces (Figure 30b). Both models predicted important damage development at the clamped region for 5.5 mm deflection as expected, but the damage state in the foil with rough interfaces is more severe, involving cracks penetrating the U-10Mo core. Figure 31 illustrates an example of an experimental single U-Mo foil sample showing cracks propagating in the U-Mo core from the asperities and/or microvoids located along an interface.

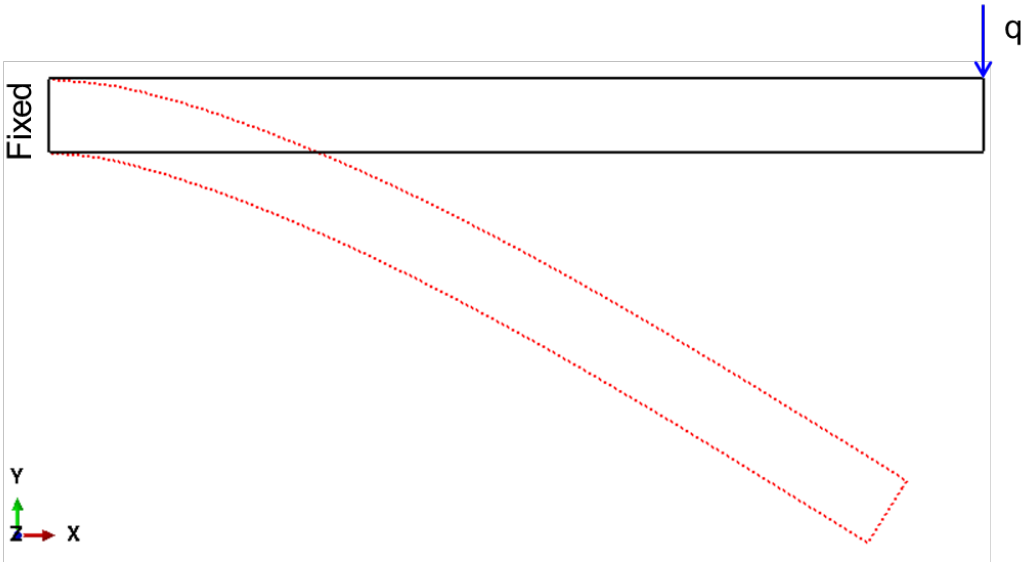

Figure 27. Boundary Conditions Applied to Deform the Al/Zr/U-10Mo Foil According to a Cantilever Beam Configuration. An increasing deflection, *q*, was applied at one end while the other end was fixed.

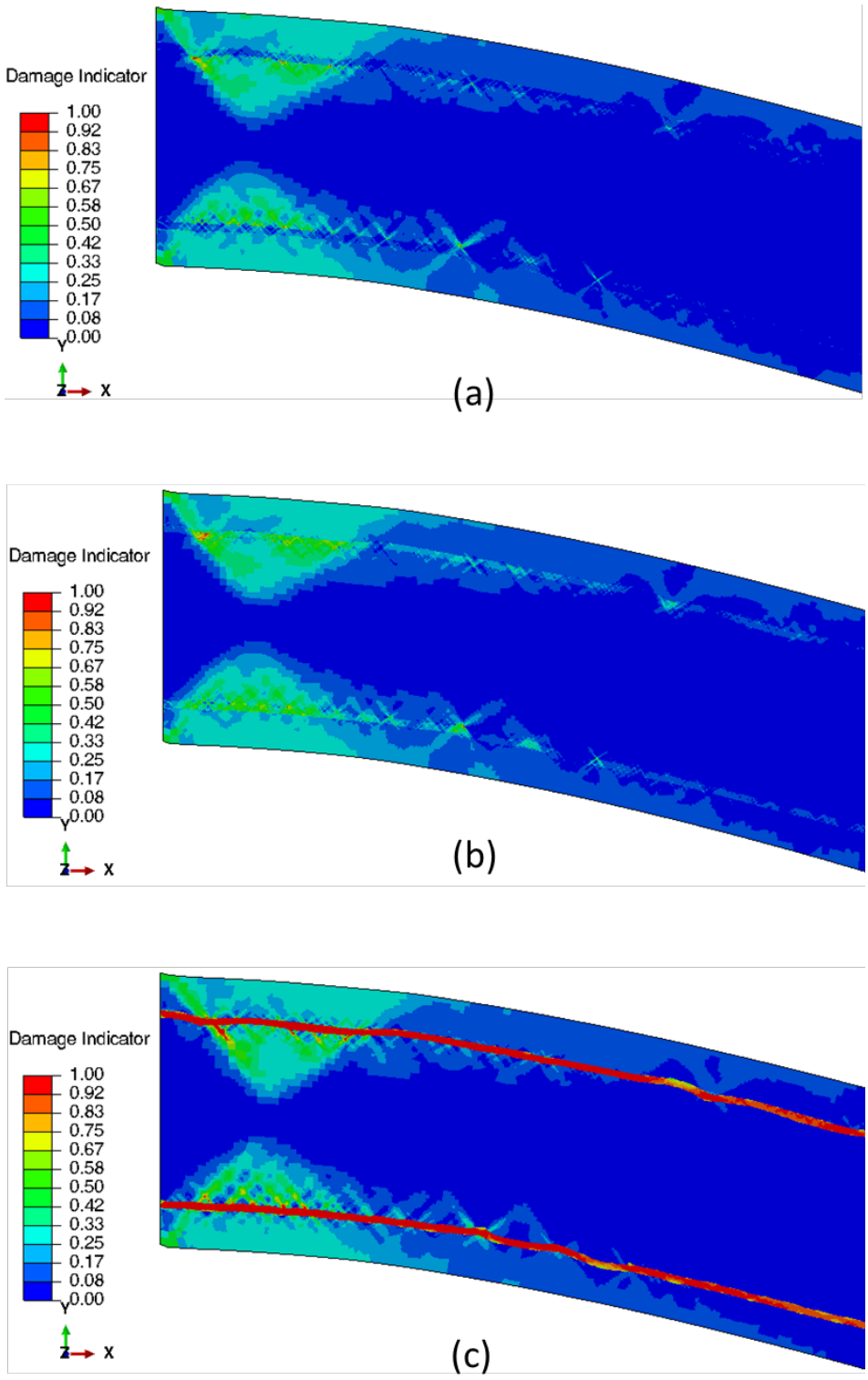

Figure 28. Snapshots of the Damage Distributions at the Clamped End Region Predicted by the Model with Interface Roughness for 4.5 mm Deflection: Analysis for (a) Zr(1), (b) Zr(2), and Zr(3)

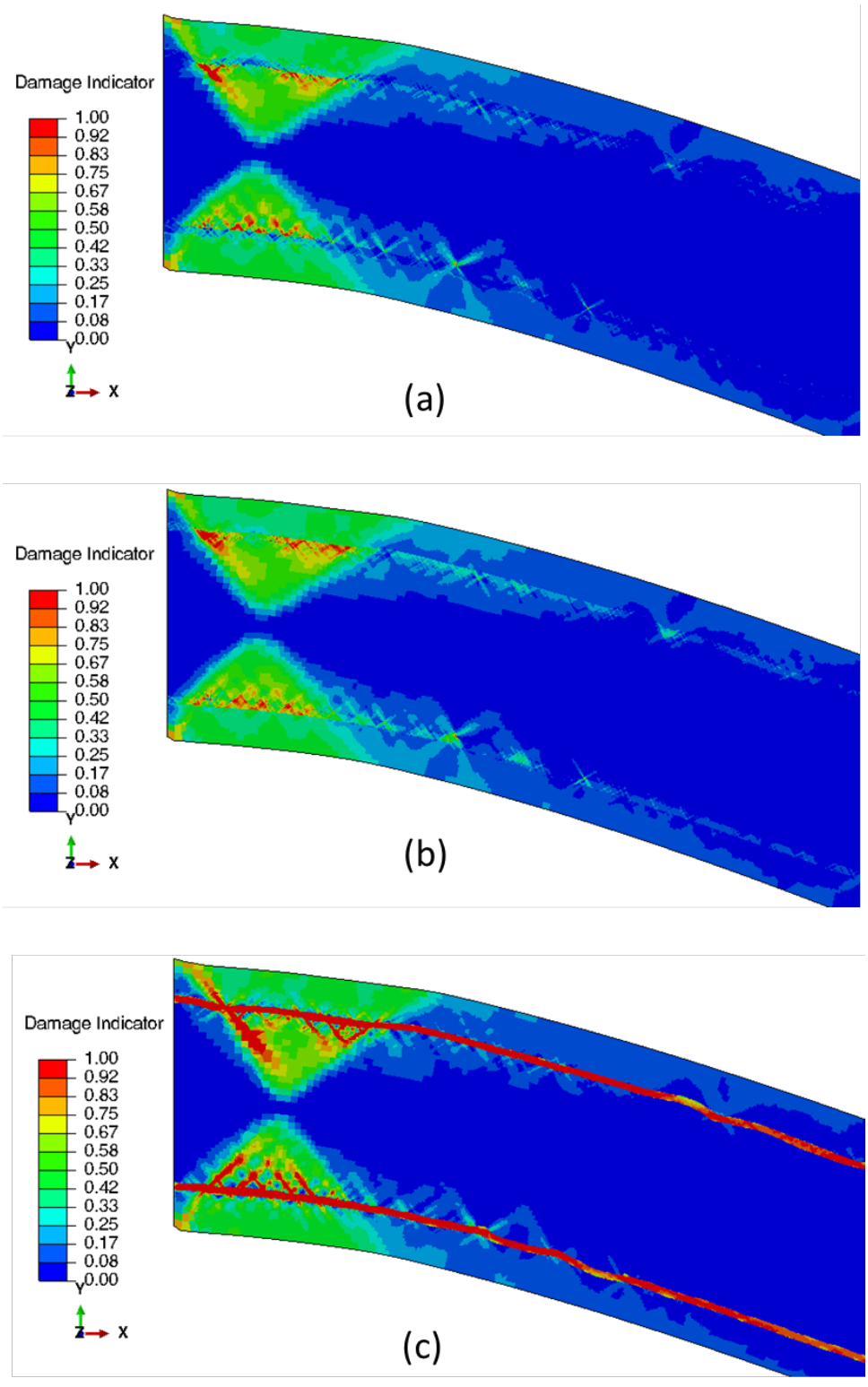

Figure 29. Snapshots of the Damage Distributions at the Clamped End Region Predicted by the Model with Interface Roughness for 5.5 mm Deflection: Analysis for (a) Zr(1), (b) Zr(2), and Zr(3)

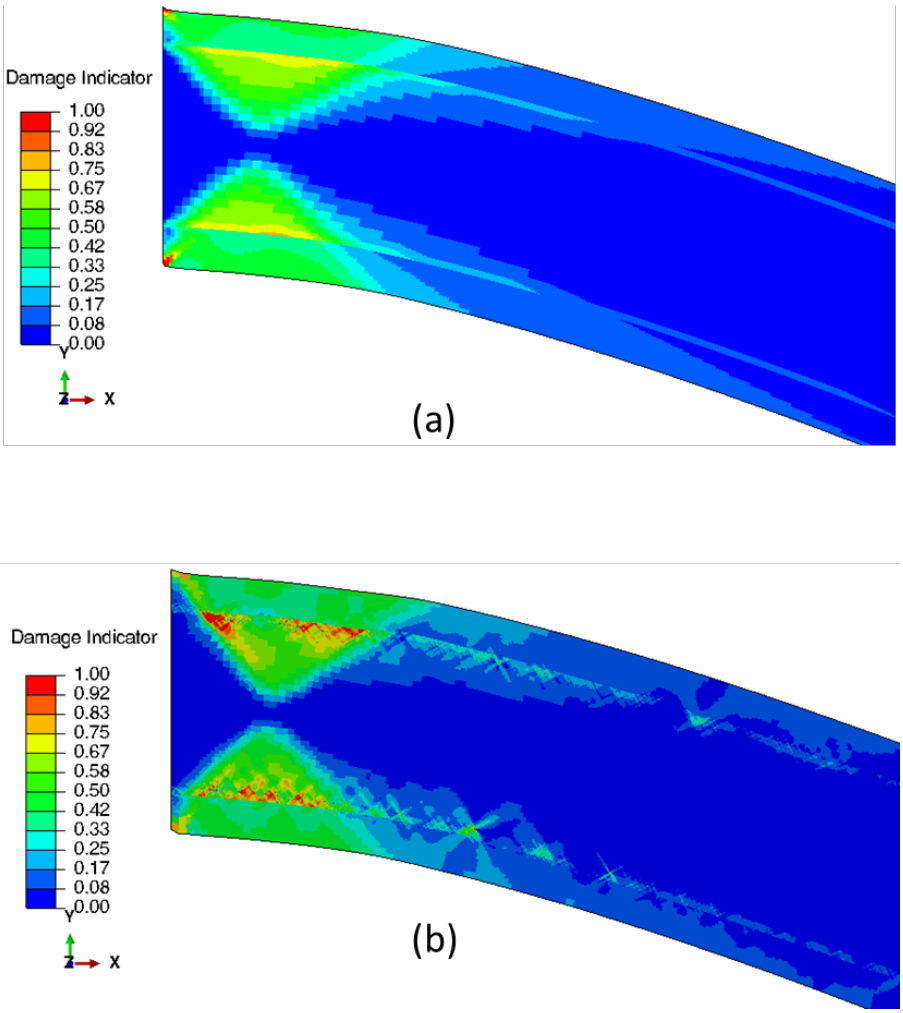

Figure 30. Snapshots of the Damage Distributions at the Clamped Region Predicted by the Models with (a) Smooth Interfaces and (b) Rough Interfaces for 5.5 mm Deflection. The analyses used material Zr(2) for the Zr layers.

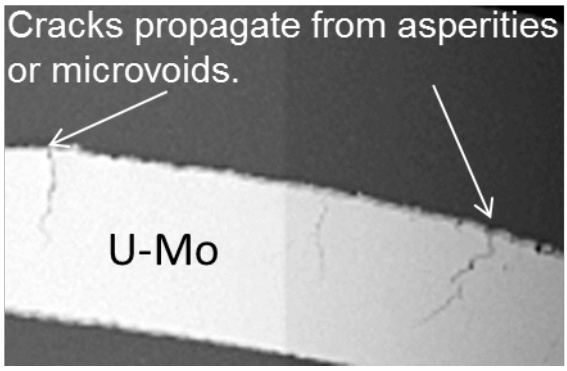

Figure 31. Example from an Experimental U-Mo Sample Showing Cracks Propagating from Asperities or Microvoids at an Interface

5.0 Conclusions

This document reports in detail the results of the sensitivity analyses performed on Al/Zr/U-10Mo foil FE damage models with smooth and rough interfaces subjected to uniform bending or a cantilever beam bending configuration. In the uniform bending configuration, the foil curvature radius of 76.58 mm after *springback* was used as an analysis criterion. The analyses used combined published and assumed constitutive mechanical data for the constituent layers. In addition, by exploring Pacific Northwest National Laboratory's Vickers hardness data for Zr with different levels of O_2 content, and considering three possible behaviors of Zr covering the range from nearly zero to high O_2 contents, a conceptual envelope of the stress-strain responses of Zr was proposed and used in the analyses. The analyses also assumed that all the layers were perfectly bonded initially. An elastic-plastic damage model with isotropic hardening and isotropic damage using ABAQUS constitutive laws was developed to simulate the deformation of the foil models subjected to bending. The foil models with smooth interfaces considered four thickness values for the Zr layers (i.e., 4, 10, 25, and 37 microns). Based on a microstructural image and using NIST's OOF2 software, a foil model with rough interfaces was developed to study the effect of the interface asperities on the foil's mechanical response and integrity.

The conclusions drawn from this work are as follows:

- *The Zr stress-strain behavior* has an important effect on foil's deformation and integrity. The very *high strength* but *brittle* Zr due to high O_2 contents (Zr(3) material) induced very high stresses to cause failure of the Zr layers. For Zr(3), higher stress concentrations were also found along the interfaces between the Zr and U-10Mo layers causing plastic deformation in these regions, although the U-10Mo core away from the interfaces was still elastic. The ductility of Zr (Zr(1) or Zr(2) materials) is an important parameter for reducing stress concentrations, and thus for improving the foil's integrity and deformation behavior. A more ductile Zr layer improves foil performance relative to shaping.
- *The effect of the Zr-layer thickness* on the stress and strain distributions is more significant at springback than at the maximum applied moments. However, for the values of the Zr thickness considered, the effect of Zr thickness appears to be less important than the effects of the Zr mechanical properties and interface roughness, and therefore should not be a concern for foil fabrication.
- Interface roughness has an important impact on foil's integrity, because the analyses for a model with rough interfaces shows that the asperities along the interfaces are sites of stress, strain, and damage concentrations. Under a critical loading mode (e.g., cantilever beam loading), damage localization in these sites could develop into microcracks propagating in the U-10Mo core. Therefore, minimizing the interface roughness would improve the foil's mechanical integrity. This modeling was not able to determine an acceptable range for interface roughness.

Because the sensitivity analyses performed under this effort used assumed or published data in model foils, the results have indicative or qualitative values. However, the modeling capability established can be enhanced and used to simulate actual tests based on measured data that could be planned for the next steps to effectively guide foil fabrication.

6.0 References

Burkes DE, R Prabhakaran, J-F Jue, and FJ Rice. 2009. "Mechanical properties of DU-xMo alloys with x = 7 to 12 weight percent." *Metallurgical and Materials Transactions A* 40(5):1069–1079. DOI: 10.1007/s11661-009-9805-5. Accessed July12, 2017, at http://link.springer.com/article/10.1007%2Fs11661-009-9805-5.

Cahoon JR, WH Broughton, AR Kutzak. 1971. "The Determination of Yield Strength from Hardness Measurements." *Metallurgical Transactions* 2(7):1979–1983. Accessed August 5, 2017, at https://link.springer.com/article/10.1007/BF02913433.

Dassault Systèmes. 2016. SIMULIA Abaqus, Dassault Systèmes Simulia Corp., Vélizy-Villacoublay, France.

Lloyd R. 2013. *Evaluation of 6061 Al Alloy Mechanical Properties of HIP-Bonded Fuel Plate Cladding: HIP-Bonded Fuel Plates*. ID TEV-1758, Idaho National Laboratory, Idaho Falls, Idaho.

Rest J, YS Kim, GL Hofman, MK Meyer, and SL Hayes. 2009. *U-Mo Fuels Handbook.* ANL-09/31, Argonne National Laboratory, Lemont, Illinois. Accessed July 31, 2017, at http://www.ipd.anl.gov/anlpubs/2009/12/65696.pdf.

Tabor D. 1951. "The hardness and strength of metals." *Journal Institute of Metals* 79:1–18.

Distribution

No. of
Copies

Name
Organization
Address
City, State and ZIP Code

Organization
Address
City, State and ZIP Code
Name
Name
Name
Name
Name (#)

Name
Organization
Address
City, State and ZIP Code

No. of
Copies

 # Foreign Distribution

Name
Organization
Address
Address line 2
COUNTRY

 # Local Distribution

Pacific Northwest National Laboratory

Name	Mailstop
Name	Mailstop
Name	Mailstop
Name	Mailstop
Name	(PDF)

Pacific Northwest
NATIONAL LABORATORY

Proudly Operated by **Battelle** *Since 1965*

U.S. DEPARTMENT OF
ENERGY

902 Battelle Boulevard
P.O. Box 999
Richland, WA 99352
1-888-375-PNNL (7665)

www.pnnl.gov